Helsinki University of Technology Radio Laboratory Publications
Teknillisen korkeakoulun Radiolaboratorion julkaisuja
Espoo, 2005 REPORT S 273

ADVANCED SPHERICAL ANTENNA MEASUREMENTS

Tommi Laitinen

Dissertation for the degree of Doctor of Science in Technology to be presented with due permission for public examination and debate in Auditorium S3 at Helsinki University of Technology (Espoo, Finland) on the 15$^{\text{th}}$ of December 2005, at 12 o'clock noon.

Helsinki University of Technology
Department of Electrical and Communications Engineering
Radio Laboratory

Teknillinen korkeakoulu
Sähkö- ja tietoliikennetekniikan osasto
Radiolaboratorio

Author: Tommi Laitinen

Title of thesis: Advanced spherical antenna measurements
Finnish title: Kehittyneet pallomaiset antennimittaukset
Date: 15th December, 2005 **Pages:** 63

Department: Department of Electrical and Communications Engineering
Chair: S-26 Radio Engineering

Supervisor: Professor Pertti Vainikainen
Instructor: Professor Pertti Vainikainen

Concrete guidelines for effectively performing spherical antenna measurements and for designing multi-probe systems will be provided. The work will mainly be restricted to antennas whose maximum cross-section dimension is in the order of 1-2 λ or less. Specific design guidelines for a very fast radiation pattern measurement system for mobile phone models will be provided. Information on practical aspects related to such a system will be provided by building a demonstrator system and testing it.

Firstly, the errors in the total radiated power and the maximum electric field are illustrated by simulations of near-zone spherical antenna measurements of electrically relatively small AUTs (antennas under test) for various applied truncation numbers and for different measurement distances [P1]. Secondly, a novel iterative matrix method is presented that is shown to provide, for a fixed relatively small number field samples, a lower uncertainty in the determination of the radiated field of an AUT model than the traditional matrix method [P2]. Thirdly, it is shown that, for a fixed relatively small number field samples, the radiation pattern can generally be determined with a lower uncertainty from the complex data than the amplitude-only data [P3]. It is shown in [P4] that a high-order probe correction becomes increasingly significant with an increasing ratio between the radius of the minimum sphere of the AUT and the measurement distance.

It is shown in [P5] that by enclosing the head phantom with a mobile phone inside the minimum sphere, and the calculation of the truncation number for the spherical wave expansion of the radiated field based on the radius of this minimum sphere in wavelengths, leads to an overestimation of the truncation number. It is illustrated by simulations for a mobile phone that by multiplying the truncation number for the mobile phone without a head phantom by a factor of approximately 1.2 leads to a reasonable truncation number for the mobile phone with the head phantom. It is demonstrated in [P6], by building and testing a spherical fully 3-D measurement system for mobile phone models (RAMS), that the radiation pattern of a typically-sized mobile phone model at approximately 1.8 GHz can be determined without its rotation with a relatively small uncertainty from the complex-valued signals gathered from only 32 dual-port probes on a spherical surface. Information on the reflectivity level inside RAMS will be provided. It is shown in [P7] that the complex radiation pattern of a mobile phone model can be determined without taking advantage of the field-disturbing radio-frequency feed cable to the mobile phone model during the measurement.

It is shown in [P8] that, instead of a single spherical wave expansion, the use of multiple spherical wave expansions (MSWE) for the field characterization can lead to a smaller number required spherical modes for reaching a desired level of uncertainty in the determination of the radiation pattern. It will further be shown, that using the MSWE technique can also lead to the smaller number of required measurement locations.

Keywords: Spherical antenna measurement, mobile phone, radiation pattern, spherical wave expansion, probe correction

Preface

Firstly, I would like to first thank my supervisor, Professor Pertti Vainikainen. During several years of research work under his supervision, I have learned to respect his honesty, objectivity and scientific leadership. His genuine interest in every single research topic he works with has motivated me significantly in my own research. Needless to say, I feel I have had a true privilege to work with him, and a unique possibility to learn under his supervision.

Secondly, I would like to thank all my co-authors and other people from the Radio Laboratory at Helsinki University of Technology, who have participated in the work reported in this thesis. In particular, I would like to thank those involved in the work with RAMS, e.g. J. Toivanen, C. Icheln, J. Ollikainen, A. Karttunen, J. Berenguer, E. Kahra, V. Sibakov, etc. Special thanks for E. Kahra and H. Frestadius for providing many high-quality figures for this thesis. I also would like to thank all other colleagues and co-workers from the Radio Laboratory for making every day a nice working day.

Thirdly, I would like to thank my present colleagues from the Electromagnetic Systems section at Technical University of Denmark, especially O. Breinbjerg, S. Pivnenko, and J. M. Nielsen, for creating an inspiring atmosphere for working with the probe correction in spherical near-field antenna measurements. Undoubtedly, the work in the Technical University of Denmark has influenced positively and significantly on this thesis.

Finally, I would like to thank my wife Anna not only for supporting me in my research but also for keeping me firmly in touch with the life outside research, which indeed exists.

Espoo, 15$^{\text{th}}$ December, 2005

Tommi Laitinen

List of Original Publications

[P1] T. Laitinen, P. Vainikainen, "Number of spherical wave modes required for the prediction of radiated EMI," *Antenna Measurement Techniques Association, 21th Annual Meeting and Symposium (AMTA'99)*, Monterey Bay, CA, USA, Oct. 4-8 1999, pp. 425-430.

[P2] T. Laitinen, P. Vainikainen, T. Koskinen, "Far-field measurements for mobile phones with a small number of measurement locations," *Electron. Lett.*, Vol. 37, No. 20, 2001, pp. 1255-1256.

[P3] T. Laitinen, P. Vainikainen, T. Koskinen, O. Kivekäs, "Amplitude-only and complex field measurements for characterizing radiated fields of mobile terminal antennas from a small number of samples," *IEEE Transactions on Instrumentation and Measurement*, Vol. 54, No. 5, Oct. 2005, pp. 1989-1996.

[P4] T. A. Laitinen, J. M. Nielsen, S. Pivnenko, O. Breinbjerg, "Errors of first-order probe correction for higher-order probes in spherical near-field antenna measurements," *URSI International Symposium on Electromagnetic Theory*, Pisa, Italy, May 23-27 2004, pp. 588-590.

[P5] T. Laitinen, P. Vainikainen, T. Koskinen, "Influence of phantom head on measurements of radiated fields of mobile phones," *Electron. Lett.*, Vol. 37, No. 5, 2001, pp. 292-293.

[P6] T. A. Laitinen, J. Ollikainen, C. Icheln, P. Vainikainen, "Rapid spherical field measurement system for mobile terminal antennas," *IEEE Instrumentation and Measurement Technology Conference (IMTC'03)*, Vail, CO, USA, May 20-22 2003, pp. 968-972.

[P7] T. Laitinen, J. Toivanen, C. Icheln, P. Vainikainen, "Spherical measurement system for determination of complex radiation patterns of mobile terminals," *Electron. Lett.*, Vol. 40, No. 22, 2004, pp. 1392-1394.

[P8] T. Laitinen, P. Vainikainen, T. Koskinen, "Multiple spherical wave expansions to characterise radiated fields of mobile phones," *Journees Internationales de Nice sur les Antennes (JINA'02)*, Nice, France, Nov. 12-14 2002, pp. 23-26.

Contribution of the author

The author has the main contributions to publications [P1]-[P8]. The author has performed the problem formulation for each publication, mostly written all the publications, and analyzed mostly the results of each publication. P. Vainikainen has been in a revisory role in publications [P1]-[P3] and [P5]-[P8].

The author has performed all the calculations for publication [P1].

The author has performed all the calculations for publications [P2], [P3], [P5] and [P8] from the simulation data of the radiated field of the mobile phone model provided by either T. Koskinen or O. Kivekäs.

The author has performed all the calculations for publication [P4]. S. Pivnenko and O. Breinbjerg have been in a revisory role in publication [P4]. J. M. Nielsen has provided help in verifying the correctness of the computer codes used for publication [P4].

The author has performed all the calculations for publication [P6] from the existing simulation data of the radiated field of a mobile phone model with a head phantom originally provided by T. Koskinen. The author has been in the leading role in planning of the rapid antenna measurement system (RAMS). The author has also performed the calculation of the far field from the measured signals obtained by RAMS. The author has participated in and instructed the calibration of RAMS and the measurements of the radiated fields of the mobile phone model with RAMS.

The idea of using the amplitude-only measurements and the phase-retrieval network in publication [P7] originated from the author. The author has also programmed the phase-retrieval algorithm used in RAMS. The author has been in the leading role in designing the radio-frequency system of RAMS operating in the spectrum analyzer mode. The author has participated in and instructed the measurements of the radiated fields of the mobile phone model with RAMS.

Contents

Chapter 1

Introduction

1.1 Scope

An antenna may be considered as a transition device between a guided wave and an unguided medium. In many applications antennas enable a more effective data transfer from one place to another than the transmission lines [1]. In other applications antennas constitute an indispensable part of the system. Examples of systems where antennas are used are e.g. mobile communication systems, radar applications, amateur radio systems etc. [1].

It is useful to know how antennas radiate in practically any application they are used. Very often, exclusively the far-field radiation characteristics of antennas are of interest. Depending on the application, important radiation parameters may be the total radiated power, the gain, the directivity, side-lobe levels, directions of null radiation, polarization properties, the efficiency, etc. [2].

The far-field radiation properties of antennas may naturally be determined by a conventional far-field measurement or using some other standard test methods [3]. An example of another technique for determining the far-field radiation properties of antennas is the near-field technique [4]. A near-field technique relies on the use of a near-field to far-field transformation for the calculation of the far field from the measured near-field signals. The measurement geometry influences on the applied near-field to far-field transformation. Typical geometries are planar, cylindrical and spherical [4]. Several other known techniques for the determination of the radiation properties of antennas will be briefly discussed later in Chapter 2 of this thesis.

The work reported in this thesis touches upon spherical near-field and far-field antenna measurements. The research will be focused on the spherical measurement geometry, because it both enables a convenient application of the well-known spherical wave expansion technique for the field characterization [5], and offers an attractive possibility for an effective determination of the radiated fields of especially of mobile phones [6].

1.2 Objectives and contents

From the scientific point of view, the work of this thesis can be roughly divided into three parts. Selected studies on spherical antenna measurements will be reported in the first part. Rapid radiation pattern measurements for mobile phone models will be dealt with in the second part. A novel field characterization technique using multiple spherical wave expansions will be introduced in the third part.

In the first part, the purpose will be to deliver information and guidelines for an effective characterization of the radiated fields, and for effectively performing spherical antenna measurements. The emphasis will be on electrically relatively small antennas whose maximum cross-section dimension is in the order of 1-2 wavelengths or less.

An examination on the measurements of the radiated fields in the near zone of an antenna is first conducted in [P1]. This study gives specific information on the required number of measurement locations for the determination of the radiated field and total radiated power with a certain reasonable uncertainty from the measured near-zone complex field. Secondly, a novel iterative matrix method for the field characterization from a very small number of complex field samples is presented in [P2]. Thirdly, methods for the characterization of the radiated fields from a small number of amplitude-only and complex (amplitude and phase) field samples are compared with the aim of providing information about an effective method for characterizing radiated fields in [P3]. Furthermore, the importance of probe correction in spherical near-field antenna measurements is briefly touched upon in [P4].

In the second part, the purpose will be to deliver both theoretical and experimental information about the measurements of the radiation properties of mobile phone models with a spherical fully 3-D multi-probe measurement system. More specifically, the aims will be 1) to show that the radiation pattern of a typically-sized mobile phone at approximately 1.8 GHz can be determined with a fully 3-D spherical measurement system with only 64 radio-frequency channels without a rotation of the mobile phone model, 2) to provide information on the reflectivity level inside such a system, and 3) to demonstrate the possibility for complex field determination without using the field-disturbing radio-frequency feed cable to the mobile phone model during the measurement.

Simulations are first carried out to produce information on the necessary number of probes required to reach a desired level of uncertainty in the determination of the total radiated power and the radiation pattern in [P5]-[P6]. This is performed for a mobile phone with and without a head phantom. Based on the simulation results, a 3-D spherical multi-probe demonstrator system will be built for the frequency of 1.8 GHz, which allows the determination of the radiation pattern of a mobile phone without a rotation of the mobile phone during the measurement [P6]-[P7]. This type of a 3-D system makes very fast radiation pattern measurements of mobile phone models possible. Furthermore, the capability of the system to retrieve the phase of the radiated field from the amplitude-only measurements is demonstrated in [P7]. The presented system allows to fully avoid the disturbing influence of the feed cable in the determination complex radiated field of mobile phone models [7] [8]. Complex field information is useful in existing and future mobile communication

systems exploiting more than one antenna in the mobile phone. Examples of such systems are the diversity [9] and the multiple-input multiple-output (MIMO) [10] systems.

Finally, a novel field characterization technique, where multiple spherical wave expansions are used, will be presented in the third part. This technique, namely the multiple spherical wave expansions (MSWE) technique, is introduced in [P1]. This study shows that taking advantage of multiple spherical wave expansions can lead to a smaller total number of spherical functions required for the field characterization with a certain degree of uncertainty compared to using a single spherical wave expansion. In this thesis, it will further be shown that the application of the MSWE technique also can lead to a smaller total number of required measurement locations.

This chapter (Chapter 1) is devoted to introduction. In Chapter 2 various antenna measurement techniques will be first briefly presented. In Chapter 3 the theory of the spherical antenna measurements will be presented. In Chapter 4 advanced spherical antenna measurements will be discussed. Here, the scientific contribution of this thesis will also be presented. Summary of the publications and conclusions will be given in Chapters 5 and 6, respectively.

1.3 Scientific contribution

The work is comprised of publications [P1]-[P8], and it delivers new and significant scientific information as follows:

Publications [P1]-[P3], [P5]-[P6] and [P8]: Concrete guidelines for effective ways, mostly in terms of the reasonable number of measurement locations, of determining radiated spherical fields of electrically relatively small radiating devices, and especially mobile phones, are delivered.

Publication [P4]: New information about the significance of probe correction in spherical near-field antenna measurements is delivered.

Publication [P5]-[P7]: Design guidelines, produced both by computer simulations and practical demonstrations, for a very fast complex radiation pattern measurement system for mobile phone models with and without the head phantom are delivered. A demonstrator system for mobile phones in built, tested and reported in [P6] and [P7]. Such a system is shown to be operable in the vector network analyzer (VNA) mode and in the spectrum analyzer mode. A feasible way of determining the complex radiation pattern of a mobile phone model from the amplitude-only measurements with the spectrum analyzer without using a radio-frequency feed cable to the mobile phone model is demonstrated at 1.8 GHz. Importantly, the applied phase-retrieval technique may obviously be used e.g. for GSM mobile phones operating in their normal operating mode. Furthermore, detailed information on the reflectivity level and the operating mode uncertainty of the system will be delivered in this thesis.

Chapter 2

Antenna measurements

Antenna measurements are discussed in general in this chapter. First, two basic concepts related to antenna measurements, the near field and the far field, will be introduced in Section 2.1. Various known techniques for measuring radiation parameters of antennas will be then briefly discussed in Sections 2.2-2.7.

It is noted at this point, that the time dependence of the electromagnetic field in the equations presented in this thesis is assumed to be $e^{-i\omega t}$, where t is time and ω is the angular frequency. This term will be suppressed from the equations.

2.1 Near and far fields

The field radiated by an antenna under test (AUT) may be divided into reactive near field, radiating near field, and far field [2]. This indicative division is based on the properties of the radiated field as a function of distance.

The reactive near field is that part of the field which is closest to the AUT. Definitions of the distance to which the reactive near field extends may be several. According to one common definition, the reactive near field extents to the distance

$$r_1 = \frac{\lambda}{2\pi}, \tag{2.1}$$

where λ is the wavelength. At this distance the amplitudes of the reactive and radiating parts of the tangential electric field of a magnetic Hertzian dipole moment are equal. The same applies for the amplitudes of the reactive and radiating parts of the tangential magnetic field of an electric Hertzian dipole moment [2]. The distance given by Eq. (2.1) is sometimes considered as the far-field distance as well.

According to another common definition, the limit between the radiating near field and the far field is at the distance

$$r_2 = \frac{2D^2}{\lambda}, \tag{2.2}$$

where D is the maximum cross-section dimension of the AUT. The distance r_2 is

also known as the Rayleigh distance [5], and it corresponds to the maximum phase error of 22.5° at the edge of the aperture of the antenna with respect to the center of the antenna [11].

In Fig. 2.1 the division of the field into the three regions according to Eqs. (2.1) and (2.2) is illustrated. Eqs. (2.1) and (2.1) are only indicative, and they have to be applied with care. Eq. (2.2) may not be useful for a small ratio between the D and λ, because in that case the reactive near field according to Eq. (2.1) extends to the far field according to Eq. (2.2), i.e. $r_1 > r_2$.

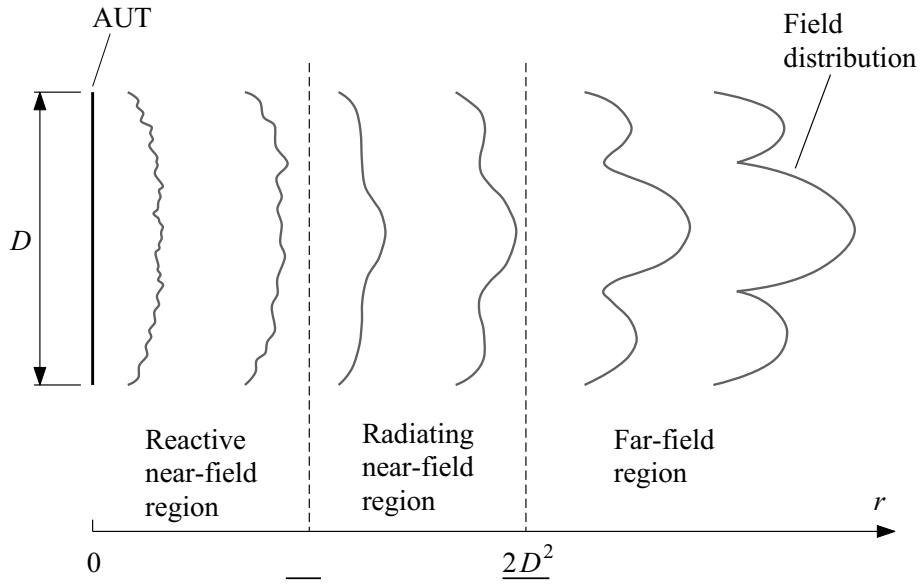

Figure 2.1: The regions of the reactive near field, the radiating near field, and the far field are illustrated as a function of distance [12].

In order to solve this problem with electrically very small antennas another useful equation for the far-field limit is

$$r_3 = \max(\frac{2D^2}{\lambda}, \frac{\lambda}{2\pi}), \tag{2.3}$$

where the Eqs. (2.1) and (2.2) have been combined into a single equation.

2.2 Conventional far-field measurement

The purpose of an antenna measurement is most often to determine the far-field characteristics of the AUT. A straight-forward method for the determination of the far-field characteristics is to perform a conventional frequency-domain far-field antenna measurement. A usual way to do this has been to rotate the AUT, depending on the application, around one or two axes, and use a single probe either to receive or transmit the measurement signal.

A natural advantage of the conventional far-field measurement, compared to e.g. the near-field technique, that will be discussed in the following section, is that the far

field is obtained directly without using a near-field to far-field transformation. On the other hand, the far-field distance may be hundreds of meters or more in some applications [11], and this can make the far-field measurement disadvantageous.

The need for fast and inexpensive methods for the determination of the far-field characteristics of AUTs has been a driving force for the development of various advanced antenna measurement techniques, to replace the conventional frequency-domain far-field measurement. Some of the most commonly used techniques will be reviewed in the following sections.

2.3 Near-field techniques

A near-field measurement is an attractive alternative to the conventional far-field measurement if the far-field distance is large. Since the signals are gathered in the near field of the AUT, a near-field to far-field transformation is required to determine the far field. The three typical near-field scanning techniques are the planar, the cylindrical and the spherical techniques [4], and they are briefly discussed in the following.

The planar technique is applicable especially for an AUT with a directive radiation pattern. The advantage of the planar technique over the cylindrical or the spherical techniques is the near-field to far-field transformation, which is commonly considered mathematically the least demanding among the three techniques. For many applications, the disadvantage of the planar technique is that it does not provide the far field in all directions, but only in a half space at maximum. The planar near-field technique has been applied e.g. in [13].

The cylindrical technique is useful e.g. for an AUT, whose radiation pattern particularly in the elevation angles around 90° is of interest. The set-up of the cylindrical scanning range is relatively simple, because only one rotation for the AUT combined with a vertically movable probe is required. The cylindrical near-field technique has been applied e.g. in [14].

The spherical technique is well-suited for applications where the radiation pattern of the AUT is of interest in all directions. The near-field to far-field transformation for the spherical technique is commonly considered slightly more mathematically demanding than that for the planar or the cylindrical technique. An advantage of the spherical geometry compared to the planar and the cylindrical geometries is related to spacial truncation [15]. The samples obtained on an appropriate spherical scanning grid constitute discrete periodic data series both in the elevation angle and the azimuthal angle, so that the truncation of the data series can be treated conveniently [5]. The theory of the spherical technique will be discussed in more detail later in Chapter 3.

2.4 Multi-probe systems

The time required for the determination of the 3-D radiation pattern of an AUT is greatly influenced by the number of required measurement directions when using

a single probe. Multi-probe systems enable to speed up the measurements [16]. A multi-probe system for the radiation pattern measurements for wireless applications is presented in [6]. The probes are located on an arch, and the AUT is rotated around one axis. Further, multi-probe systems are presented for testing of vehicle mounted antennas in [17], and for testing especially mobile phones in [18]. All these techniques rely on the rotation of the AUT during the measurement.

A fully 3-D multi-probe system is proposed in [19]. An actual implementation of this type of a system is presented in [P6] and [P7]. These fully 3-D multi-probe systems allow, for an AUT of a certain electrical size, the measurement of the radiation pattern without a rotation or a movement of the AUT. This offers possibilities for a practically real-time radiation pattern measurement, and thus a possibility to evaluate e.g. instantaneous radiated fields of mobile phones. In Fig. 2.2 a spherical, fully 3-D radiation pattern measurement system is illustrated.

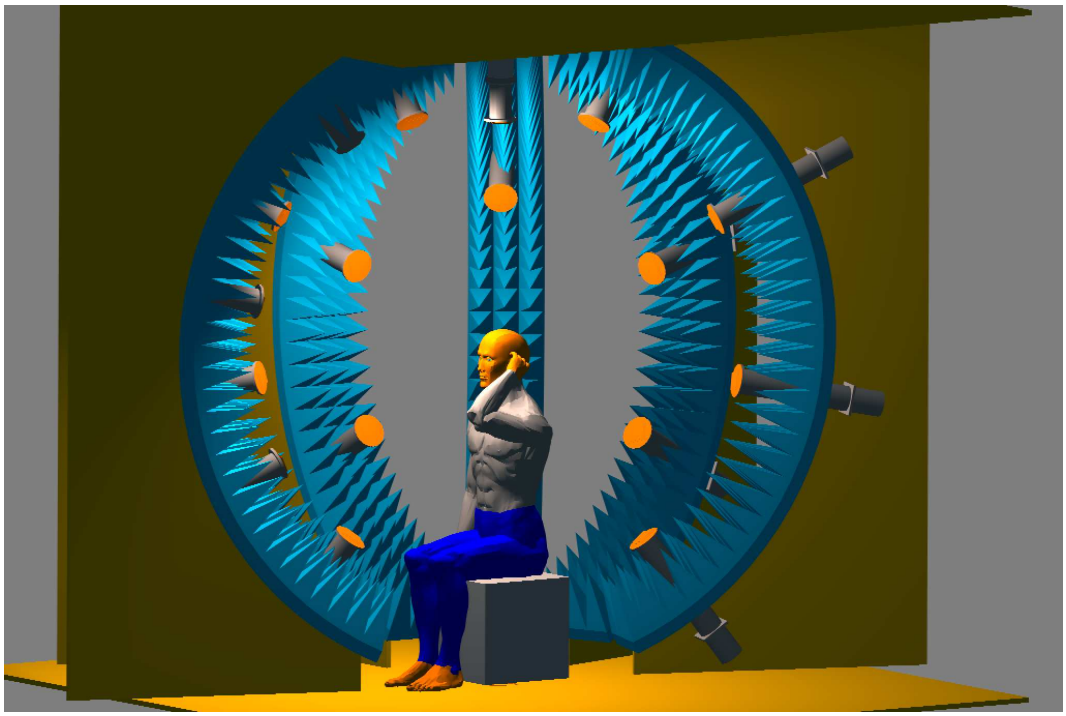

Figure 2.2: Illustration of a fully 3-D spherical spherical antenna measurement system.

2.5 Compact range techniques

Compact range techniques exploit a specific mechanical structure to convert an initial spherical radiated field to a plane wave, so that the AUT can be tested in far-field conditions. The far-field environment is created in a relatively small space, and the near-field to far-field transformation is not required. The collimating device, that transforms a spherical wave to a plane wave, can be a reflector, a lens or a hologram, of which the most commonly used is the reflector [20]. The function of a compact range based on a reflector is illustrated in Fig. 2.3.

Using a compact range the far-field characteristics in one plane are obtained by

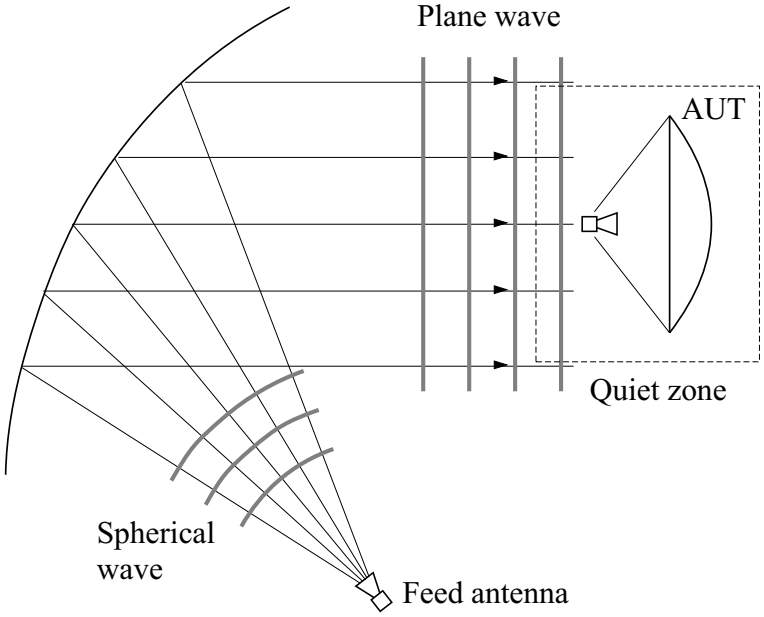

Figure 2.3: The idea of a compact antenna test range based on a reflector is illustrated. The reflector converts an initial spherical wave to a plane wave.

a single rotation of the AUT, which is its advantage compared to e.g the near-field technique. One of the challenges of the compact range is the reduction of the influence of the edge diffraction of the collimating device on the quiet zone field [21] [22].

2.6 Time-domain techniques

Antenna measurements may be performed in the time domain. In the time-domain measurement the AUT is fed with a pulse, and the signal is measured with a digital sampling oscilloscope. The frequency response of the AUT may be obtained via a Fourier transform. This corresponds to the situation where the AUT is excited with different frequency components over a certain region of frequencies at the same time [23].

The time-domain measurement can be clearly advantageous over the frequency-domain measurement for its short measurement time in such applications where the radiation properties of an AUT are desired over a large frequency range. The time-domain measurement further provides possibilities to filter out multiple reflections between AUT and the probe and the reflections from the surroundings [23]. In this way a low-cost chamber could be used for antenna measurements. Time-domain formulations of the near-field scanning e.g. for planar and spherical geometries are presented in [24] and [25], respectively.

2.7 Other techniques

A Wheeler cap, a reverberating chamber, and a gigahertz transverse electromagnetic (GTEM) cell are examples of other environments, where radiation properties of AUTs can be measured and evaluated [26]. The Wheeler cap can be used for the determination of the efficiency of the AUT [27]. The measurements of the performance of a mobile terminal antenna in a reverberating chamber (or a mode-stirred chamber) is reported in [28]. In particular, it is pointed out that the reverberating chambers may be used for the characterizing diversity properties of mobile terminal antennas [29]. The GTEM cell is proposed for testing radiation characteristics of small AUTs in [30]. The reverberating chamber and the GTEM cell are recognized also in the standards of electromagnetic compatibility [31].

Chapter 3

Spherical antenna measurement theory

The theory of spherical antenna measurements will be presented in this chapter. This theory is based on the use of the spherical wave expansion [5], and it is applicable for both the spherical near-field and far-field antenna measurements.

The spherical vector wave expansion will first be presented in Section 3.1. Definitions for several important radiation parameters will then be given in Section 3.2. The formulation of the spherical measurement problem will be presented in Section 3.3, and its solution discussed in Section 3.4.

3.1 Spherical vector wave expansion

The spherical vector wave expansion of electromagnetic fields was presumably first introduced in [32]. Later this expansion has been applied widely for characterizing radiated fields by the spherical antenna measurements, e.g. in [5] [33]. A general outward propagating vectorial electric field radiated by an AUT in the spherical coordinates can be expressed as an infinite series of spherical vector wave functions as [5]

$$\boldsymbol{E}(r,\theta,\varphi) = \frac{k}{\sqrt{\eta}} \sum_{s=1}^{2} \sum_{n=1}^{\infty} \sum_{m=-n}^{n} Q_{smn} \boldsymbol{F}_{smn}^{(3)}(r,\theta,\varphi), \tag{3.1}$$

where $\boldsymbol{E}$ is the outward propagating electric field, (r,θ,φ) are the standard spherical coordinates, k is the wave number, η is the intrinsic admittance of the measurement medium, Q_{smn} are the spherical vector wave coefficients (Q coefficients), and $\boldsymbol{F}_{smn}^{(3)}(r,\theta,\varphi)$ are the power-normalized spherical vector wave functions [5].

According to the well-known empirical rule [5], the spherical vector wave series can be truncated at certain $n = N$ ($N = 1, 2...$), where the truncation number is

$$N = [kr_0] + n_1, \tag{3.2}$$

where n_1 is an integer, and r_0 is the radius of the minimum sphere that fully encloses the AUT, and the square brackets provide the smallest integer greater than

or equal to the number inside the square brackets. Depending on the application, and the requirement for the accuracy of the field characterization, n_1 varies. Commonly, n_1=10 is considered sufficient for all practical purposes [5], and especially for electrically small antennas.

A practical, truncated form of Eq. (3.1) is

$$\boldsymbol{E}(r,\theta,\varphi) = \frac{k}{\sqrt{\eta}} \sum_{s=1}^{2} \sum_{n=1}^{N} \sum_{m=-n}^{n} Q_{smn} \boldsymbol{F}_{smn}^{(3)}(r,\theta,\varphi). \tag{3.3}$$

The electric field at a large distance may thus be approximated as [5]

$$\boldsymbol{E}(r,\theta,\varphi) = \frac{k}{\sqrt{\eta}} \frac{1}{\sqrt{4\pi}} \frac{e^{ikr}}{kr} \sum_{s=1}^{2} \sum_{n=1}^{N} \sum_{m=-n}^{n} Q_{smn} \boldsymbol{K}_{smn}(\theta,\varphi), \tag{3.4}$$

where the far-field pattern functions $\boldsymbol{K}_{smn}(\theta,\varphi)$ are [5]

$$\boldsymbol{K}_{smn}(\theta,\varphi) = \lim_{kr\to\infty} [\sqrt{4\pi} \frac{kr}{e^{ikr}} \boldsymbol{F}_{smn}^{(3)}(r,\theta,\varphi)]. \tag{3.5}$$

It is seen from Eq. (3.1), that the radiated field is completely determined by the Q coefficients of the spherical wave expansion. The Q coefficients may further be expressed as $Q_{smn} = vT_{smn}$, where v is the input signal to the AUT, and T_{smn} are the transmission coefficients of the radiated field [5]. The v, T_{smn} and the far-field pattern functions $\boldsymbol{K}_{smn}(\theta,\varphi)$ are presented here, because they can be used to determine many essential parameters of the radiated field, as will be presented later in Section 3.2.

The only truncation that has been assumed in Eqs. (3.3) and (3.4), and that will be assumed later in the forthcoming Sections 3.2-3.3, concerns the presented n-mode truncation. Another practical truncation rule concerns the m-mode truncation. The azimuthal mode index m may be truncated at certain $|m| = M < N$, where M is the truncation number for the m index of the spherical wave expansion [5]. The M may be found from

$$M = [kr_c] + n_2, \tag{3.6}$$

where r_c is the radius of the minimum circular cylinder parallel to the z axis completely enclosing the AUT, and n_2 is again a number specific for the application and the required field characterization accuracy [5]. Typically, $n_2 = 10$ should be sufficient for all practical purposes.

The truncated form of Eq. (3.1) now becomes

$$\boldsymbol{E}(r,\theta,\varphi) = \frac{k}{\sqrt{\eta}} \sum_{s=1}^{2} \sum_{n=1}^{N} \sum_{m=-\min(n,M)}^{\min(n,M)} Q_{smn} \boldsymbol{F}_{smn}^{(3)}(r,\theta,\varphi), \tag{3.7}$$

where both the n and m-mode truncations have been assumed. In this equation, the M may assume values from 0 to N.

For later purposes Eq. (3.7) is further expressed as

$$\boldsymbol{E}(r,\theta,\varphi) = \frac{k}{\sqrt{\eta}} \sum_{j=1}^{J} Q_j \boldsymbol{F}_j^{(3)}(r,\theta,\varphi), \tag{3.8}$$

where the summation over the indices (s, m, n) has been replaced by the summation over the index j only. For $n = 1...N$, for $m = -\min(n, M)...\min(n, M)$, and for $s = 1, 2$, the index j becomes

$$j = 2(n(n+1) + m - 1) + s - \frac{1}{2}(|n - M| + n - M)^2. \tag{3.9}$$

The total number of modes in the spherical wave characterization is

$$J = 2M(M+2) + 2(2M+1)(N-M). \tag{3.10}$$

In such a case, where only the n-mode truncation is assumed ($M = N$), Eqs. (3.9) and (3.10) reduce to those presented in [5]: $j = 2(n(n+1) + m - 1) + s$, and $J = 2N(N+2)$, respectively.

3.2 Radiation parameters

In this section equations for some important and useful parameters of the radiated field are presented in terms of the Q coefficients of the radiated field, the input signal v, and the transmission coefficients. It is here assumed that $M = N$.

The total radiated power, in terms of the Q coefficients, is [5]

$$P = \frac{1}{2}\sum_{s=1}^{2}\sum_{n=1}^{N}\sum_{m=-n}^{n}|Q_{smn}|^2. \tag{3.11}$$

The directivity is [5]

$$D(\theta, \varphi) = \frac{1}{2P}\left|\sum_{s=1}^{2}\sum_{n=1}^{N}\sum_{m=-n}^{n}Q_{smn}\boldsymbol{K}_{smn}(\theta, \varphi)\right|^2. \tag{3.12}$$

The gain is [5]

$$G(\theta, \varphi) = \frac{\frac{1}{2}\left|\sum_{s=1}^{2}\sum_{n=1}^{N}\sum_{m=-n}^{n}Q_{smn}\boldsymbol{K}_{smn}(\theta, \varphi)\right|^2}{\frac{1}{2}|v|^2(1 - |\tau|^2)}, \tag{3.13}$$

where τ is the voltage reflection coefficient of the antenna. For $\tau = 0$ the power incident at the antenna $P_{inc} = \frac{1}{2}|v|^2$ thus equals the power accepted by the antenna $P_{in} = \frac{1}{2}|v|^2(1 - |\tau|^2)$. For a lossless antenna, and for $\tau = 0$, the total radiated power becomes $\frac{1}{2}|v|^2$.

The power radiated by the modes for a fixed n is of general interest. The so-called n-mode power spectrum, $P_{rad}^{(n)}$, is useful for analyzing the cut-off property of the spherical wave modes as a function of n. The $P_{rad}^{(n)}$ expresses the power radiated by all the spherical wave modes with the same index n for $n = 1, 2..N$ [5]. The n-mode power spectrum is

$$P_{rad}^{(n)} = \frac{1}{2}\sum_{s=1}^{2}\sum_{m=-n}^{n}|Q_{smn}|^2. \tag{3.14}$$

The normalized n-mode power spectrum, $P_{rad,norm}^{(n)}$ is determined from the $P_{rad}^{(n)}$ by setting the maximum value of the spectrum to 0 dB.

3.3 Spherical measurement problem

Spherical antenna measurements are performed to gather information of the radiated field of the AUT for its characterization. A spherical antenna measurement is a natural choice for many applications because it offers both a practical measurement geometry and a possibility for a convenient mathematical formulation of the problem. In a typical spherical antenna measurement, the radiated field of the AUT is expressed in terms of the spherical vector wave functions, and the desired unknowns are the Q coefficients of the AUT field.

In spherical antenna measurements, essentially, the relation between the signal received by the probe and the input signal to the AUT is recorded, which for a given frequency, is a complex number. This relation depends e.g. on the measurement distance and the direction, the polarization of the probe, the radiated spherical wave modes of the AUT, the probe reception properties, and the disturbance fields from the surroundings.

Three significantly different approaches for formulating the spherical antenna measurement problem will be discussed in this thesis. In the most general approach, that will be discussed in Section 3.3.1, the disturbance fields are assumed present in the test zone. These disturbance fields are generated e.g. by the reflections from the surroundings. This approach, namely the test-zone field compensation approach [34], includes both the conventional probe correction [5], and the compensation for the disturbance fields. In the second approach, that will be discussed in Section 3.3.2, the disturbance fields are assumed negligible, and only the conventional probe correction is performed. This approach, namely the free space approach with probe correction, is the conventional probe correction approach described e.g. in [5]. The third approach, namely the free space approach without probe correction will be dealt with in Section 3.3.3, and it concerns an important special case where an electric Hertzian dipole is used as a probe in free space conditions. This approach is important because it is closely related to the spherical far-field measurements in general.

3.3.1 Test-zone field compensation approach

In the test-zone field compensation approach [34], both the direct signal from the AUT and the disturbance fields from the surroundings are assumed present at the probe in the spherical antenna measurement. The idea is to establish a relationship between each outward-propagating spherical mode in the test zone of the AUT and the signal received by the range antenna (probe) by a separate test-zone field (TZF) calibration measurement. In this measurement a known TZF calibration probe is rotated and translated on a spherical surface enclosing the test volume, and the transmission signal is recorded for each polarization of the range antenna, and for each position and orientation of the TZF calibration probe. The data obtained by the test-zone calibration measurement can be used to determine the desired test-zone coefficients. These coefficients are comparable to the probe receiving coefficients in the conventional spherical near-field antenna measurements [5], but in addition to correcting for the influence of the probe, they can also be used to compensate the influence of the disturbance fields from the surroundings.

An iterative solution for the compensation of the disturbance fields, that includes the correction for the probe, is also presented in [34]. Importantly, the presented solution is computationally efficient, and may therefore be used for electrically relatively large AUTs.

Since the publication of [34], the test-zone field compensation has been worked with e.g. in [35]. The application of the test-zone field compensation for multi-probe systems is very briefly touched upon later in Chapter 4 of this thesis.

3.3.2 Free space approach with probe correction

A common trend in the antenna measurement community has been to build anechoic chambers of high enough quality to suppress the disturbance fields in the test zone, e.g. the reflected fields from the walls. It is then typically assumed that the disturbance fields in the test zone are negligible, and only the direct line of sight signal is significant. In this case, with the known receiving pattern of the probe, an analytical relation between the desired Q coefficients of the radiated field of the AUT and signal received by the probe can be established. This relation is called the transmission formula.

The probe-corrected transmission formula for the spherical near-field antenna measurements was first derived in [36]. Since then another type of transmission formula has been proposed in [37]. Of these two, the transmission formula presented in [36] is presumably more commonly-used. Complete formulation of the spherical near-field antenna measurements applying this transmission formula is presented in [5]. In this thesis only the transmission formula presented in [5] is considered, and its derivation explained. For this purpose the spherical measurement coordinates are now described.

The spherical measurement coordinate systems are illustrated in Fig. 3.1. The AUT and the probe coordinate systems are the unprimed and the primed coordinate systems, respectively. The origin of the primed coordinate system in the unprimed coordinate system is defined by the standard spherical coordinates (r, θ, φ) of the unprimed coordinate system [3]. Minimum spheres enclosing the AUT and the probe, with radii r_0 and r_0', respectively, are shown. The probe is constantly pointing to the origin of the unprimed coordinate system. The probe orientation is defined by the probe rotation angle (χ), so that for $\chi = 0^\circ$ and $\chi = 90^\circ$ the x' axis is coinciding with the θ and φ unit vectors of the unprimed coordinate system, respectively [5].

The spherical scanning takes place by rotating the unprimed coordinate system relative to the primed coordinate system, i.e. by changing the values of the θ, φ and χ coordinates. The measurement distance r is constant during the scan. It is noted, that using a dual-polarized probe, whose ports are identical correspond to the situation where the scanning with a single-polarized antenna takes place for $\chi = 0^\circ$ and $\chi = 90^\circ$.

It is noted at this point that the Eqs. (3.2)-(3.3), that are valid for the AUT in the unprimed coordinate system, are also valid for the probe in the primed coordinate system by replacing the indices (s, m, n) by indices (σ, μ, ν), the coordinates (r, θ, φ) by coordinates (r', θ', φ'), r_0 by r_0', N by ν_{max}, and by replacing the Q coefficients

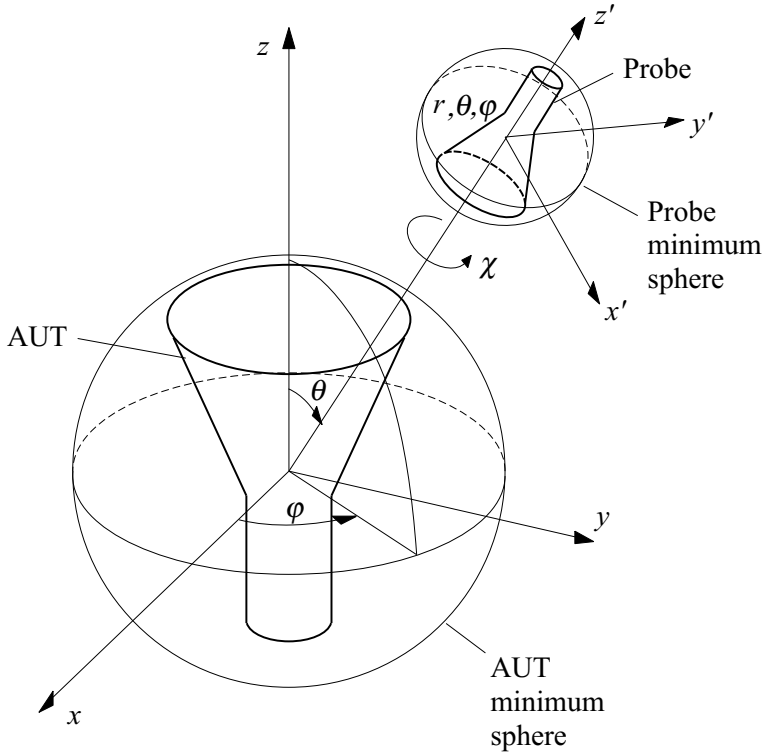

Figure 3.1: Spherical measurement configuration.

of the AUT by the Q coefficients of the probe $Q'_{\sigma\mu\nu}$. These notations mostly follow those used in [5].

The derivation of the transmission formula as presented in [5] may now be explained with the help of Fig. 3.1. The radiated field of the probe and the AUT are first expressed in terms of the spherical vector wave modes using Eqs. (3.2)-(3.3). The probe receiving coefficients are determined from the Q coefficients of the probe by assuming a reciprocal probe [5]. Then, the spherical vector wave functions, describing the outward-propagating field radiated by the AUT, are rotated and translated, using the translation addition theorem for the spherical vector wave functions [38] [39], so that the initial outward-propagating spherical waves in the unprimed coordinate system are expressed in terms of the inward and outward-propagating spherical waves in the primed coordinate system [5]. Now, the probe is introduced in the primed coordinate system, and it is assumed, that this introduction does not change the currents of the AUT, that is, multiple reflections between the AUT and the probe are assumed negligible. Finally, the coefficients of the inward-propagating spherical waves in the primed coordinate system are multiplied appropriately with the receiving coefficients of the probe to form the transmission formula for the received signal [5]. In this way, the transmission formula becomes [5]

$$w(r,\chi,\theta,\varphi) = \sum_{s=1}^{2}\sum_{n=1}^{N}\sum_{m=-n}^{n}\sum_{\mu=-\mu_0}^{\mu_0} Q_{smn}P_{s\mu n}(kr)e^{i\mu\chi}d^n_{\mu m}(\theta)e^{im\varphi}, \tag{3.15}$$

where w is a complex-valued signal received by the probe, $\mu_0 = \min(n, \nu_{max})$, $P_{s\mu n}(kr)$ are the probe response constants, and $e^{i\mu\chi}$, $d^n_{\mu m}(\theta)$, and $e^{im\varphi}$ are the rotation coefficients [5]. The probe response constants and the rotation coefficient

$d^n_{\mu m}(\theta)$ are defined in [5]. The probe response constants can be calculated from the probe receiving coefficients.

In conclusion, the spherical measurement problem with conventional probe correction has been set now, and the aim is to find the unknown Q coefficients of Eq. (3.15). This will be discussed later in Section 3.4.

3.3.3 Free space approach without probe correction

When the probe correction is not applied, it is commonly assumed that the signal received by the probe is proportional to the tangential electric field on a spherical measurement surface. In fact, this assumption would be valid if an electric Hertzian dipole were used as a probe.

It is now considered that a tangential, x'-oriented electric Hertzian dipole is used to sample the radiated field on a spherical surface. In this case, the signal received by the dipole (w^e) as a function of the χ angle and the electric field at the dipole becomes [5]

$$w(r,\chi,\theta,\varphi) = \frac{\sqrt{6\pi\eta}}{2k}\boldsymbol{E}(r,\theta,\varphi)\cdot[\cos(\chi)\boldsymbol{u}_\theta + \sin(\chi)\boldsymbol{u}_\phi], \tag{3.16}$$

where Eqs. (3.45)-(3.46) in [5] are combined to a single equation.

Inserting Eq. (3.3) into Eq. (3.16) leads to the transmission formula for the electric Hertzian dipole [5]

$$w^e(r,\chi,\theta,\varphi) = \frac{\sqrt{6\pi}}{2}\sum_{s=1}^{2}\sum_{n=1}^{N}\sum_{m=-n}^{n} Q_{smn}\boldsymbol{F}^{(3)}_{smn}(r,\theta,\varphi)\cdot[\cos(\chi)\boldsymbol{u}_\theta + \sin(\chi)\boldsymbol{u}_\phi]. \tag{3.17}$$

Eq. (3.17) may also be understood as a transmission formula for the spherical (near-field) antenna measurements without probe correction. Its solutions is discussed in the following section.

3.4 Inverse problem

In the spherical antenna measurements, when the spherical wave expansion is used for the characterization of the radiated field, the purpose is to find the unknown Q coefficients of the AUT. The Q coefficients may then be used for calculating many important radiation parameters, as shown in Section 3.2. In order to find the gain certain additional measures have to be taken [5].

It will be shown in this section, how the Q coefficients of the AUT field can be found. Solutions to the Q coefficients of the AUT field using the test-zone field compensation approach [34] will not be discussed here. The discussion will thus be restricted to the free-space approaches with and without the probe correction. In the free space approach with probe correction the Q coefficients are found by solving the transmission formula (3.15). This thus provides the probe-corrected solution for the Q coefficients of the AUT. In the free space approach without probe correction

either the spherical wave expansion (3.3) or the transmission formula for an electric Hertzian dipole (3.17) can be used to find the Q coefficients.

In Section 3.4.1 the analytical solutions for the transmission formulas with and without probe correction will be presented [5]. In Section 3.4.2 discrete solutions for finding the Q coefficients will be discussed.

3.4.1 Analytical solution

The analytical solution for the Q coefficients here assumes that a continuous received signal on a spherical measurement surface is available. Then by taking advantage of the orthogonality integrals for the rotation coefficients $e^{i\mu\chi}$, $d^n_{\mu m}(\theta)$, and $e^{im\varphi}$ of the transmission formula (3.15) [5], this can be written into form

$$Q_{1mn}P_{1\mu n}(kr) + Q_{2mn}P_{2\mu n}(kr) = w^n_{\mu m}(r), \tag{3.18}$$

where the terms $w^n_{\mu m}(r)$ can be found from the orthogonality integral [5]

$$w^n_{\mu m}(r) = \frac{2n+1}{8\pi^2}\int_{\theta=0}^{\pi}\int_{\varphi=0}^{2\pi}\int_{\chi=0}^{2\pi} w(r,\chi,\theta,\varphi)e^{-i\mu\chi}e^{-im\phi}d^n_{\mu m}(\theta)\sin(\theta)d\chi d\varphi d\theta. \tag{3.19}$$

Here, Eqs. (4.45), (4.48) and (4.51) in [5] have been used. Noticeably, the orthogonality integral of Eq. (3.19) shows, that, in general, the received signal must be available, not only as a function of θ and φ angles, but also as a function of χ angle. This means, that performing the probe correction in a general case by taking advantage of the orthogonality of all three rotation coefficients in this way requires the probe rotation during the measurement.

However, it is known, that for a first-order ($\mu = \pm 1$) probe, for which the azimuthal (φ') dependence of the receiving field can be accurately expressed in terms of the exponential function $e^{i\mu\varphi'}$ by restricting $\mu = \pm 1$, the Q coefficients of the AUT can be found from Eqs. (3.18) and (3.19) using only two probe orientation angles during the measurement of the AUT [40] [41] [42]. This is the idea of the well-known, computationally efficient first-order ($\mu = \pm 1$) probe correction technique described in [5].

If the probe correction is not required, the transmission formula for the electric Hertzian dipole can be used, and the solution for the Q coefficients can be written as

$$Q_{smn} = a_{smn}(kr)\int_{\theta=0}^{\pi}\int_{\phi=0}^{2\pi}[w^e(r,0,\theta,\varphi)\boldsymbol{u}_\theta + w^e(r,\frac{\pi}{2},\theta,\varphi)\boldsymbol{u}_\varphi] \cdot \boldsymbol{F}^{(3)}_{s-mn}(r,\theta,\varphi)\sin(\theta)d\varphi d\theta. \tag{3.20}$$

Here $a_{smn}(kr) = \frac{2}{\sqrt{6\pi}}(-1)^m[\frac{1}{R^{(3)}_{sn}(kr)}]^2$, where $R^{(3)}_{sn}(kr)$ is either the spherical Hankel function ($s = 1$) or a function derivable from the spherical Hankel function ($s = 2$) as defined in [5].

3.4.2 Discrete solution

In practice, the received signal is available only for a finite number of measurement directions (θ,φ), and for a finite number of probe orientations (χ). A number of methods have been presented for finding the unknown Q coefficients from a discrete set of measured data, both for the case, where the probe correction is not taken into account [43], and where it is taken into account [44]. To the author's knowledge, the two most commonly used techniques are the matrix method and the Fourier transform technique [43]. A combination of these two techniques has also been proposed in [44], and recently in [45]. The matrix and the Fourier transform methods will be described, and some of their advantages and disadvantages briefly discussed in the following.

Matrix method

The matrix method for finding the Q coefficients of the spherical wave expansion is presented in [43] for the case where the probe correction is not taken into account. Yet, the matrix method is applicable to the probe-corrected case as well [5] [44]. In the matrix method, the spherical wave expansion (without probe correction) or the transmission formula (with probe correction) is written in a form of a matrix, so that for each combination of angles θ, φ and χ, an equation between the known received signal and the unknown Q coefficients of the AUT is written. Solving this matrix equation thus provides all the Q coefficients simultaneously, provided the angles θ, φ and χ are chosen appropriately. The choice of the measurement locations should allow a formation of a matrix with a sufficient number of linearly independent rows. If the number of equations is greater than the number of desired Q coefficients, the matrix equation may be solved by pseudo-inversion [46]. The pseudo-inversion for finding the Q coefficients of the AUT has been applied e.g. in [P3] and [47].

For later purposes, the matrix method for solving the Q coefficients will be now mathematically described for the case without probe correction. It is assumed that the radiated electric field of an AUT has been measured for θ and φ polarizations at measurement locations (r, θ_l, φ_l), where index $l = 1...L$, and L is the total number of measurement locations. The purpose is now to find the Q coefficients related to the radiated field from Eq. (3.8) using the matrix method.

Electric field vector is formed as follows:

$$\bar{E} = \begin{bmatrix} \bar{E}_\theta \\ \bar{E}_\varphi \end{bmatrix}. \tag{3.21}$$

Here $\bar{E}_\alpha = [\boldsymbol{E}(r, \theta_1, \varphi_1)\boldsymbol{u}_\alpha, ..., \boldsymbol{E}(r, \theta_L, \varphi_L)\boldsymbol{u}_\alpha]^{\mathrm{T}}$, where $\boldsymbol{u}_\alpha$ is the α unit vector, and α is either θ or φ, and $^{\mathrm{T}}$ is transpose. The $\boldsymbol{E}(r, \theta_l, \varphi_l)\boldsymbol{u}_\alpha$ thus represents the measured electric field component in α polarization at measurement location l.

Matrix $\bar{\bar{F}}$ is

$$\bar{\bar{F}} = \begin{bmatrix} \bar{\bar{F}}_\theta \\ \bar{\bar{F}}_\varphi \end{bmatrix}, \tag{3.22}$$

where

$$\bar{\bar{F}}_\alpha = \frac{k}{\sqrt{\eta}} \begin{bmatrix} \boldsymbol{F}_1^{(3)}(r,\theta_1,\varphi_1)\boldsymbol{u}_\alpha & \dots & \boldsymbol{F}_J^{(3)}(r,\theta_1,\varphi_1)\boldsymbol{u}_\alpha \\ \vdots & & \vdots \\ \boldsymbol{F}_1^{(3)}(r,\theta_L,\varphi_L)\boldsymbol{u}_\alpha & \dots & \boldsymbol{F}_J^{(3)}(r,\theta_L,\varphi_L)\boldsymbol{u}_\alpha \end{bmatrix}, \tag{3.23}$$

where α is again either θ or φ. In Eq. (3.23) the spherical modes $\boldsymbol{F}_j^{(3)}(r,\theta_l,\varphi_l)$ are required for $j = 1...J$, where j and J depend on the applied truncation numbers N and M in the field characterization according to Eqs. (3.9) and (3.10), respectively.

The vector for the Q coefficients for $j = 1...J$, $\bar{Q} = [Q_1, ..., Q_J]^{\mathrm{T}}$, is now found from

$$\bar{Q} = (\bar{\bar{F}}^{\mathrm{H}}\bar{\bar{F}})^{-1}\bar{\bar{F}}^{\mathrm{H}}\bar{E}, \tag{3.24}$$

where $^{\mathrm{H}}$ is hermitian transpose. If the number of elements in $\bar{Q}$ is smaller than the number of rows in $\bar{\bar{F}}$, then this equation provides the least-squares solutions for the Q coefficients.

Fourier transform method

In the Fourier transform method the measurement directions and χ angles where the samples are recorded are equidistantly located in θ, φ and χ. By the discrete Fourier transforms of the measured signals in θ, φ and χ, and by the application of the orthogonalities of the rotation coefficients, the transmission formula (3.15) is separated into $N(N+2)$ matrix equations, where the sizes of the matrices to be inverted are now 2×2. Importantly, as previously mentioned, samples of the field are required for more than two χ values for a general probe, but two χ values are sufficient for a first-order probe. If the probe correction is not applied, the discrete Fourier transforms of the measured θ and φ components of the electric field provide the solution for the Q coefficients.

It is further noted here, that recently an iterative technique for the conventional probe correction, that is based on the use of the traditional first-order probe correction [5], has been presented in [48]. The applied iteration method is similar to that applied for the test zone field compensation in [34], but the iterative technique is now applied for the conventional probe correction [48]. This technique is computationally efficient, and also practical, because it requires only two probe orientations during the AUT measurement. The technique is shown to be applicable for more general probes than first-order probes in [49].

Advantages and disadvantages

Of these two described methods for finding the Q coefficients, an advantage of the matrix method is that it is not restricted to a regular scanning grid whereas the conventional Fourier transform method is. This means that the over-sampling factor, that is the ratio between the number of measurement samples and the number of spherical wave modes used in the characterization of the radiated field is at least approximately 2 for the conventional Fourier transform method. The over-sampling factor for the matrix method can be as low as 1. Another advantage of the matrix

method is that its practical application is generally not restricted to first-order probes, but it can also be used for general probes.

The disadvantage of the matrix method is its computational inefficiency. In a general case ($M = N$), the number of Q coefficients to be found is $2N(N+2)$, and thus with an increasing N the computational cost of the matrix method increases rapidly. In this respect, the conventional Fourier transform based first-order probe correction is both computationally efficient and practical [5].

Chapter 4

Advanced spherical antenna measurements

4.1 Brief introduction

In this chapter, aspects related to effectively performing spherical antenna measurements, as well as aspects related to design and implementation of multi-probe systems will be discussed. In order to perform spherical antenna measurements in a reasonable manner, it is important e.g. to correctly choose how to characterize the radiated field, to reasonably choose the measurement directions and the number of measurement directions, and e.g. to know when the probe correction is necessary. It may also be important to to be able to estimate if the amplitude-only measurements are sufficient for the determination of a desired field parameter. These issues are naturally significantly dependent on e.g. the desired radiation parameter, the requirement for the uncertainty of the determination of this radiation parameter, the electrical size of the AUT etc..

In this chapter, methods to determine the total radiated power and the radiation pattern of mainly such AUTs whose maximum cross-section dimension is in the order of 1-2 λ at maximum will be examined.

First miscellaneous, selected issues related to effectively performing spherical antenna measurements will be investigated in Section 4.2. These issues include e.g. the investigation on the necessary number of measurement locations and on the possibilities to reduce or minimize the number of measurement locations using an iterative matrix method, the comparison of the amplitude-only and complex field measurements, and finally, a study on the significance of probe correction.

A demonstrator system for rapid spherical antenna measurements for mobile phone models, whose design is partly based on the results of the investigations presented in Section 4.2, will be presented in Section 4.3. This system allows the determination of the radiated field of a mobile phone model without its rotation during the measurement. The system therefore provides a basis for real-time radiation pattern measurements of mobile phone models. The system further allows the complex field determination without attaching a field-disturbing radio-frequency feed cable to the mobile phone model during the measurement.

Finally in Section 4.4 a multiple spherical wave expansion (MSWE) technique is presented. It will be shown that, for some AUTs, the application of this technique enables to improve the accuracy of the characterization of the radiated field from a fixed small number of field samples.

4.2 Selected studies

In this section, several guidelines for effectively performing spherical antenna measurements will be provided. These guidelines may be applied for conventional spherical antenna measurements with a single probe, and they can also be exploited in the design of multi-probe measurement systems.

Section 4.2.1 will be devoted to examinations on the necessary number of measurement direction to be applied for spherical antenna measurements. This includes a study on a suitable truncation number [P1], and the introduction of the iterative matrix (IM) method for optimizing the number of required measurement locations [P2]. In Section 4.2.2 a comparison of the amplitude-only and complex far-field measurements with a relatively small number of measurement locations will be presented [P3]. Here the IM method presented in Section 4.2.1 will be tested against some other amplitude-only and complex field characterization techniques. In Section 4.2.3 the significance of probe correction in accurate spherical near-field antenna measurements will be discussed [P4].

4.2.1 Number of measurement directions

Spherical antenna measurements for the determination of e.g. the total radiated power and the directivity are based on gathering samples of the radiated field in different directions around the AUT. It is common for many conventional antenna measurement systems [5] [51] [52], that only one probe is used. This practically leads to a relatively long measurement time, which may then vary e.g. from half an hour to several hours depending on the measurement system and the electrical size of the AUT.

In order to at least partly overcome the problem with a relatively long measurement time using single-probe systems, multi-probe measurement systems have been developed for e.g. the measurements of the mobile terminal antennas [6]. The requirement for fast radiation pattern measurements is obviously a driving force for the development of multi-probe measurement systems also for other applications [17].

The number of directions where the samples are gathered is an issue that influences significantly on the measurement time when a single probe is used. It also influences on the cost of a multi-probe spherical measurement system. The number of measurement channels is a particularly important parameter for fully 3-D spherical measurement systems [P6].

In the following, first concrete guidelines for choosing an appropriate number of measurement directions will be given [P1], and then the idea of the IM method [P2]

will be briefly explained.

Truncation number for single-origin SWE

It is known that the number of measurement directions, where samples of the radiated field must be gathered in order to determine the radiated field with a certain degree of accuracy depends generally on the total number of spherical modes J required for the field characterization. In a general case, the number J depends on the truncation number N as $J = 2N(N+2)$ (Eq. (3.10) with $M = N$). The truncation number in turn depends generally on the electrical size of the AUT according to Eq. (3.2), where n_1 depends on the accuracy requirement.

The value $n_1 = 10$ in Eq. (3.2) is commonly considered a fair number for accurate spherical near-field antenna measurements [5]. For many practical purposes this number is impractically high. For scattering analysis some other rules for an appropriate truncation number are presented in [53]. For electrically small antennas ($kr_0 < 1$) n_1=0 is proposed in [54].

A simulation study is performed in [P1] in order to clarify in detail how the choice of n_1 influences on the uncertainty of the determination of the maximum electric far field and the total radiated power in the range $0.03 < kr_0 \leqslant 4$ for the chosen simulation model of an AUT. The radiated near-zone field of the AUT model is calculated in a relatively small number of locations. The calculated field is characterized with the spherical vector wave expansion by determining the Q coefficients of the expansion up to the truncation number N using the matrix method involving a pseudo-inversion as described in Section 3.4.2. This characterized radiated field, represented by the determined Q coefficients, is then compared with the radiated field calculated directly from the known currents of the test model. The differences in the maximum absolute values of the electric field and in the total radiated powers are determined. The results are produced for the range $0.03 < kr_0 \leqslant 4$ and for the measurement distances from $2r_0$ to approximately $27r_0$. The truncation number is varied depending on the value of kr_0, according to Eq. (3.2) by changing the value of the parameter n_1.

The results of the study performed in [P1] are briefly summarized here. For $1 < kr_0 \leqslant 4$ the results show that the errors in the total radiated power and in the absolute value of the maximum electric field for $n_1 = 0$ do not exceed 0.5 dB. Further, for $kr_0 = 4$ and for $n_1 = -1$ the same errors are always less than 1 dB. The errors for $1 < kr_0 \leqslant 4$ are generally not dependent on the measurement distance for $r \geqslant 2r_0$. For $0.03 < kr_0 < 1$ the results show that the errors in the total radiated power and in the absolute value of the maximum electric field for $n_1 = 0$ ($N = 1$) depend noticeably on the value of kr_0 at some close fixed measurement distances, e.g. for $r = 2r_0$. Both of the two errors are, however, less than 1 dB for $n_1 = 0$ for the measurement distances $r \geqslant 4r_0$. More detailed results can be found in [P1].

Iterative matrix (IM) method

In spherical antenna measurements, the origin of the spherical wave expansion is commonly placed to the origin of the minimum sphere in order to reach, in view

of Eq. (3.2), the lowest value for the truncation number N. Another possibility would be to place the origin of the spherical vector wave expansion to the assumed phase center of the AUT. If the number of spherical wave modes used for the field characterization is e.g. $N = [kr_0]$, that is $n_1 = 0$, the location of the origin of the spherical vector wave expansion relative to the location of the phase center of the AUT may have a significant influence on the accuracy of the field characterization. On the other hand, it is generally not obvious where the phase center of the AUT is located.

In [P2] the IM method is presented for performing spherical antenna measurements with a small number of measurement locations. The method is based on finding an "optimum" origin for the spherical vector wave expansion. This "optimum" origin is found in the location where the difference between the modal field and the measured field at the measurement locations is minimized. It is noted, that the idea of dislocating the origin of the spherical vector wave expansion in the near-field measurements has been proposed earlier in [55]. However, as explained in [5], the technique proposed in [55] requires that both the electric and magnetic field at the probe locations are known.

On one hand, it is shown by simulations in [P2] that the IM method method can be applied to lower the uncertainty of the field characterization compared to using a conventional matrix method. On the other hand, the IM method enables to place the AUT freely inside a certain test volume without actually increasing the required truncation number N. The method can thus be taken advantage of in situations where it is undesirable or impossible to place the origin of the spherical wave expansion to the assumed phase center of the AUT or to the origin of the minimum sphere enclosing the AUT.

A brief description of the iterative matrix method for solving the Q coefficients will now be given assuming a far-field measurement. It is thus assumed that the electric field vector as given in Eq. (3.21), representing the measured electric field components in the far field, is available. As well, the matrix $\bar{\bar{F}}$ as given in Eq. (3.22) is known.

In the matrix method described in Section 3.4.2 the over-determined equation for the Q coefficients is of the form $\bar{E} = \bar{\bar{F}}\bar{Q}$, and the least-squares solution to this equation is found from Eq. (3.24). In the IM method, the over-determined equation is

$$\bar{\bar{D}}^{(o)}\bar{E} = \bar{\bar{F}}\bar{Q}, \tag{4.1}$$

where $\bar{\bar{D}}^{(o)}$ is now a square diagonal matrix with dimension $2L \times 2L$ with diagonal elements $d_{l,l} = d_{L+l,L+l} = e^{ik(r-|\boldsymbol{r}_l-\boldsymbol{r}^{(o)}|)}$ for $l = 1...L$. Here $\boldsymbol{r}_l$ is the vector from the origin of the coordinate system to lth measurement location, and $\boldsymbol{r}^{(o)}$ (translation vector) is the vector from the origin of the coordinate system to the (translated) origin of the spherical wave expansion.

It is now possible to calculate the Q coefficient vector ($\bar{Q}^{(o)}$) related to the particular translation from Eq. (3.24) by replacing $\bar{E} \rightarrow \bar{\bar{D}}^{(o)}\bar{E}$. The residual vector $\bar{R}^{(o)} = \bar{\bar{F}}\bar{Q}^{(o)} - \bar{\bar{D}}^{(o)}\bar{E}$, related to the particular translation, is then calculated. Such $\boldsymbol{r}^{(o)}$, which minimized the square sum of the absolute values of the elements of $\bar{R}^{(o)}$, is then called the optimum $\boldsymbol{r}^{(o)}$.

The approximate value of the optimum $\boldsymbol{r}^{(o)}$ may be found iteratively, or systematically by just giving sufficient number of values for $\boldsymbol{r}^{(o)}$ inside a certain space, where the optimum $\boldsymbol{r}^{(o)}$ is known to exist. Various optimization methods exist for finding the optimum $\boldsymbol{r}^{(o)}$ iteratively [50].

It is now explained how the iteration steps are taken in [P3], the results of which will be summarized in the following section. Prior to the actual iteration steps, several initial values are set. The iteration step number p is set $p = 0$. The d_p, indicating a distance in meters after pth iteration, is set $d_0 = 0.1$ m, the $\boldsymbol{r}_p^{(o)}$, that is the best approximation of the minimum $\boldsymbol{r}_p^{(o)}$ after pth iteration, is set $\boldsymbol{r}_0^{(o)} = 0\boldsymbol{u}_x + 0\boldsymbol{u}_y + 0\boldsymbol{u}_z$.

The iterative procedure consists of the following 4 steps: 1) the iteration step number is set as follows: $p = p + 1$, 2) the distance is set as follows: $d_p = \frac{d_0}{2^{p-1}}$, 3) in total 125 vectors $\boldsymbol{r}^{(o)}$ are generated, 4) it is marked $\boldsymbol{r}_p^{(o)} = \boldsymbol{r}_{p,\min}^{(o)}$, where $\boldsymbol{r}_{p,\min}^{(o)}$ is such $\boldsymbol{r}^{(o)}$ (generated in the previous step) that gives the smallest square sum of the absolute values of the elements of the corresponding 125 residual vectors $\bar{R}^{(o)}$. The calculation of $\bar{R}^{(o)}$ is explained above.

The step number 3 is now explained in more detail. The generation of 125 vectors $\boldsymbol{r}^{(o)}$ is described by means of intersection points of 15 planes. First 5 planes are generally defined as $\gamma = -d_p + \boldsymbol{r}_{p-1}^{(o)}\boldsymbol{u}_\gamma$, $\gamma = -\frac{d_p}{2} + \boldsymbol{r}_{p-1}^{(o)}\boldsymbol{u}_\gamma$, $\gamma = \boldsymbol{r}_{p-1}^{(o)}\boldsymbol{u}_\gamma$, $\gamma = \frac{d_p}{2} + \boldsymbol{r}_{p-1}^{(o)}\boldsymbol{u}_\gamma$, and $\gamma = d_p + \boldsymbol{r}_{p-1}^{(o)}\boldsymbol{u}_\gamma$, where $\boldsymbol{u}_\gamma$ is the γ unit vector. By replacing $\gamma \rightarrow x$, $\gamma \rightarrow y$ and $\gamma \rightarrow z$, in total 15 planes are then generated. In total $5^3 = 125$ translation vectors are then defined as vectors from the center of the measurement sphere to the 125 points, where 3 of the 15 planes intersect.

The iteration steps presented above are then repeated until $p = 5$ and including the steps 2-4 for $p = 5$. For $d_0 = 0.1$ m and for $p = 5$, an uncertainty in the order of 3 mm (or less) in the location of the optimum origin of the spherical wave expansion remains. For the frequency of 2.1 GHz, that is the greatest applied frequency in the simulations carried out in [P3], this uncertainty in the location of the optimum origin has been found practically insignificant.

If the measurement locations in the application of the IM method were covering the whole spherical surface in the far field, the spherical wave theory, and in particular, the well-known spherical vector wave translations would evidently provide a relatively straight-forward theoretical justification for the functioning of the IM method. In the case the number of measurement locations is relatively small the situation is different. In this work, the function of the IM method with a small number of measurement locations has been verified in [P3] with extensive simulation series for several mobile phone models at several frequencies and with varying number of measurement locations.

4.2.2 Amplitude-only and complex field measurements

The theory presented in Chapter 3 is restricted to the characterization of complex (amplitude and phase) radiated fields of antennas from the complex-valued signals measured on a spherical surface. Several reasons for considering the complex measurements exist. Firstly, complex field is generally required for characterizing

radiated far fields from the near-field signals. Secondly, applications exist where the knowledge of the complex radiated field is useful or is required for estimating the performance of the AUT. Thirdly, the well-known (complex) spherical vector wave expansion provides a physically understandable and a practical basis for spherical antenna measurements [5]. Fourthly, the application of some techniques, e.g. the IM method described in Section 4.2.1, or the test zone field compensation discussed in Section 3.3.1 require complex field information.

In some applications, e.g. where the measurement is performed essentially in the far field, the complex field measurements may not be required nor may be desirable. In Fig. 4.1 the far-field distances according to Eqs. (2.1) and (2.2) are presented as a functions of frequency for the frequency range from 30 MHz to 5 GHz for an AUT with the maximum cross-section dimension $D = 0.2$, 0.4 and 0.8 m. It is seen from Fig. 4.1 that the far-field conditions are met with both criteria (Eq. (2.3)) e.g. for mobile phones with $D = 0.2$ m in the frequency range from 0.9 to 2.2 GHz at distances greater then 0.6 m.

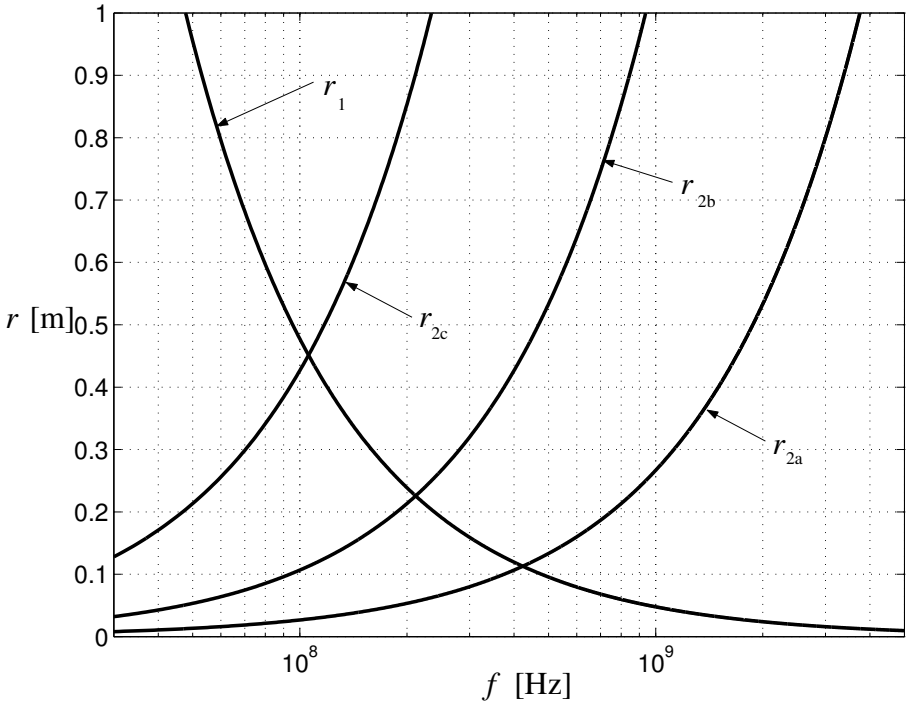

Figure 4.1: Far-field distances r_1 and r_2 as a function of frequency. The r_1 is the far-field distance according to Eq. (2.1). The r_{2a}, r_{2b} and r_{2c} are the far-field distances according to Eq. (2.2) for $D = 0.2$ m, 0.4 m and 0.8 m, respectively.

The purpose of this section is to give a summary of the comparison of the amplitude-only and complex field measurements presented in [P3]. In [P3] far-field measurements for mobile phones beside a head phantom with a relatively small number of measurement locations on a spherical surface are examined by simulations. The uncertainties in the determination of the total radiated power and the radiation pattern from the known amplitude-only and complex tangential field are illustrated. The spherical wave expansion and the Fourier expansion based techniques are compared.

The results in [P3] indicate that for a certain fixed and relatively small number

of measurement locations the complex field measurements provide the radiation pattern and the total radiated power generally with a lower uncertainty than the amplitude-only measurements. In this work the IM method, described in Section 4.2.1, is one of the applied techniques, and is shown to perform best among the compared techniques. The results in [P3] additionally provide information about a reasonable over-sampling factor to be applied in conjunction with the matrix method for solving the Q coefficients. Based on the examination in [P3] the over-sampling factor could be in the range from 1.2 to 1.6 in the noise-free case. The examinations on a reasonable over-sampling factor for the noisy case will be reported elsewhere.

4.2.3 Significance of probe correction

In general, if the signal received by the probe during the spherical antenna measurement is assumed proportional to the tangential electric field component corresponding to the polarization of the probe, so that the proportionality factor is independent on the measurement direction, the probe correction is not required. Otherwise, the theoretically correct way to find the Q coefficients is to perform the probe correction. In other words, the probe correction is not required e.g. if the scanning takes place in the far field. Also, if e.g. an electric Hertzian dipole is used as probe, regardless of the measurement distance, the probe correction is not required [5].

The first-order ($\mu = \pm 1$) probe correction technique is a commonly applied probe correction technique [5]. The importance of this probe correction for first-order probes is examined in [56], and some results are also presented in [5]. These results indicate that the probe correction is useful for accurate spherical near-field antenna measurements. However, it is shown in [56], that the first-order probe correction may not be necessary for a circular waveguide probe if the ratio ϵ between the measurement distance (r) and the radius of the minimum sphere of the AUT (r_0), $\epsilon = \frac{r}{r_0}$, is greater than 4.5.

Due to e.g. manufacturing inaccuracies, probes are never exactly first-order probes. Certain probes, e.g. an open-ended rectangular waveguide probe, approximate first-order probes to such a degree, that these probes are sometimes treated as first-order probes in spherical near-field antenna measurements [57]. In order to clarify the significance of a probe correction for more general probes than first-order probes, the errors due to the application of the first-order ($\mu = \pm 1$) probe correction for more general probes is examined in [P4]. The main result of this examination is that the errors generally increase with a decreasing ratio of ϵ. For approximately $\epsilon = 3$ the error in the determination of the main beam directivity of the investigated AUT model is less than 0.5 dB for many typical practical probes.

The significance of probe correction will be discussed more in the context of the design of a multi-probe measurement system for mobile phone models in the following section.

4.3 Spherical multi-probe system for hand-held mobile phones

An experimental, fully 3-D spherical measurement system for the determination of complex radiation pattern of a mobile phone model without a rotation of the mobile phone model during the measurement will be presented in this section. This type of a system is illustrated in Section 2.4. The system may not only be used used for mobile phone models, but for other electrically relatively small radiating devices as well.

First, the state of the art of the multi-probe measurement systems will be briefly discussed in Section 4.3.1. The aims of this work will be presented in Section 4.3.2. The design and implementation of the system will be described in Subsection 4.3.3 and 4.3.4, respectively. Validation and calibration measurements will be described in Section 4.3.5. Some future prospects of the system will be briefly discussed in Section 4.3.6.

4.3.1 State of the art

The most advanced commercial multi-probe antenna measurement systems of today are restricted to solutions, that in some way rely on the rotation of the mobile phone during the measurement [6] [17], and thus a real-time, fully 3-D characterization of the radiated field using these systems is not possible. Evidently, on one hand, the reason for this is the cost of the radio-frequency electronics required by the system. On the other hand, the number of required measurement channels generally increases relative to N^2 for fully 3-D systems [P6], whereas the increase is relative to N for arch-type systems relying on the rotation of the AUT during the measurement [6].

Further, in order to determine the complex radiated field, the radiation pattern measurements with existing systems typically require attaching a feed cable to the mobile phone model during the measurement. This disturbs the radiated field, and the result may not necessarily be sufficiently accurate. Complex radiated field is important e.g. in optimizing the diversity or the MIMO (multiple-input multiple-output) performance of a mobile phone.

4.3.2 Aims

The aim is firstly to demonstrate the possibility of rapid radiation pattern measurements with an experimental spherical fully 3-D measurement system for mobile phone models with a relatively small number of probes. Minimizing the number of probes is important in that the cost of the system is significantly dependent on the number of measurement channels.

The aim is secondly to demonstrate the possibility of the determination of the complex radiated fields of a mobile phone model from the measured amplitude only data without taking advantage of a radio-frequency feed cable to the mobile phone model during the measurement. This is possible using a specific switching circuitry called a phase-retrieval network (PRN). Compared to determining the amplitude of

the far field only, the determination of the complex far field provides a possibility to estimate more realistically the performance of a mobile phone model involving more than one antenna e.g. in a MIMO system by using the complex radiation pattern data of the mobile phone model together with the complex radio channel data [58]. The complex field measurements are also beneficial, compared to the amplitude-only measurements, in that they generally provide a lower uncertainty in the field characterization with a fixed, relatively small number of measurement channels [P3]. This can be important in optimizing the number of channels of a fully 3-D measurement system and thus potentially reducing the overall cost of the system. Moreover, the application of e.g. the iterative matrix method [P2] or the test-zone field compensation technique [34] require complex field information.

Furthermore, the aim is to provide, by developing the system, information on the practical problems and limiting factors related to the radiation pattern measurements of mobile phones with this type of a fully 3-D spherical multi-probe system. Here, interesting parameters are e.g. the reflectivity level inside the system, and the functioning and the uncertainty of the phase retrieval from the amplitude-only measurements.

4.3.3 Design

Truncation number

For typically-sized mobile phones of today, the values of r_0 vary approximately from 0.05 m to 0.1 m. The frequency range is approximately from 0.9 GHz to 2.2 GHz. These typical values of r_0 for the mentioned frequency range correspond approximately to the minimum and the maximum values of $[kr_0]$ of 1 and 5, respectively.

The results presented in Section 4.2.1 indicate that for $kr_0 = 4$, using $n_1 = 0$ and $n_1 = -1$ the uncertainties in the determination of the maximum radiated field and the total radiated power of the AUT are less than 0.5 dB and 1 dB, respectively. By assuming that these results for $[kr_0] = 4$ also hold for $[kr_0] = 5$, and by accepting the uncertainty of 1 dB in the total radiated power and the maximum electric field, the choice of the truncation number thus is $N = 4$.

With the truncation number $N = 4$, the number of measurement channels required by the system is at least $J = 2N(N + 2) = 48$. With an oversampling factor of e.g. $\frac{4}{3}$, which may be considered reasonable in the noise-free case [P3], the number of measurement locations becomes 64.

To verify the correctness of the choice of the truncation number, and to give an illustrative example of the cut-off of the spherical wave modes, the normalized n-mode power spectrum of a mobile phone model with 0.1 m long chassis and a helix antenna, calculated from Eq. (3.14), is presented in Fig. 4.2 for $n = 1..10$. The origin of the spherical wave expansion is in the feed point of the antenna, the frequency is 1.8 GHz, and $kr_0 \approx 4.1$, and thus $[kr_0] = 5$. It is seen that the power for $n = 5$ is less than 1 percent relative to the highest power ($n = 1$). In this case, for instance, the cumulative relative power for modes up to $n = 3$ and 4 is 96.9 and 99.6 percent, respectively.

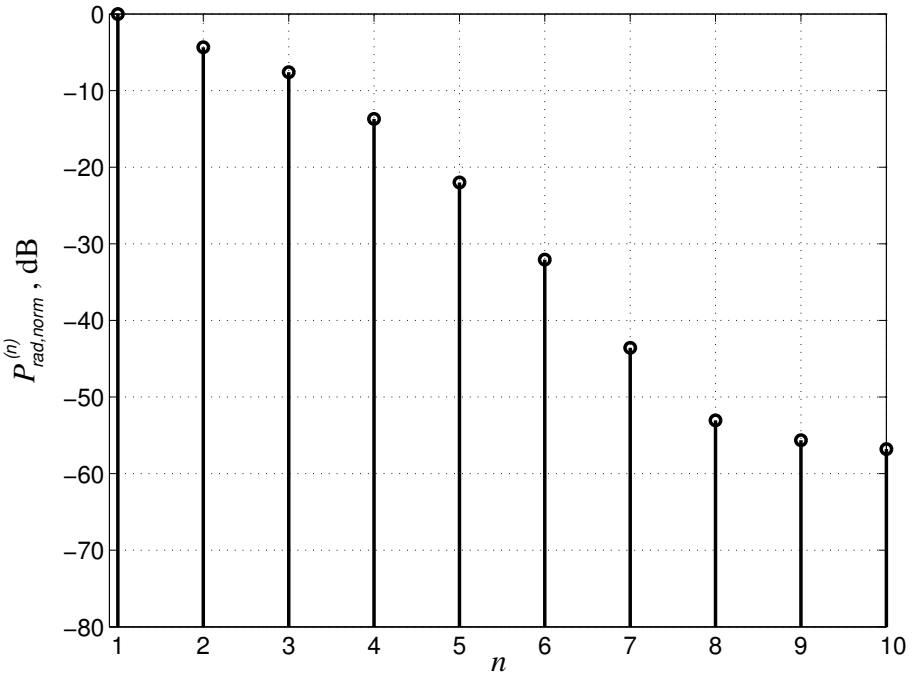

Figure 4.2: The normalized n-mode power spectrum of a mobile phone model with a 0.1 m long chassis and a helix antenna calculated from Eq. (3.14). The AUT model used here is the same as the EUT_{10} (equipment under test) in [P2]. The origin of the spherical wave expansion is in the feed point of the antenna.

Influence of head phantom

It is of interest to investigate the influence of the head phantom on the measurements of the radiated fields of mobile phones. Theoretically, the minimum sphere that fully encloses the AUT would be determined in this case essentially by the size of the head phantom. This would then inevitably lead to a relatively large truncation number and a relatively large number of measurement channels for the system.

In [P5] simulations for a model of a mobile phone with a head phantom are carried out. The results show that for such a case where all the spherical modes up to $N = 4$ are used to characterize the radiated field of a mobile phone without the head phantom, the introduction of the head phantom increases the required truncation number by a factor of approximately 1.15 in order to reach approximately the same uncertainty [P5]. It is thus estimated based on the results of these simulations that the introduction of a head phantom does not influence on the radiated field of the mobile phones in such a way that the required N to characterize the radiated field should be changed so significantly as the minimum sphere analysis would indicate.

Mutual interaction between probes in a multi-probe system

It is obvious that errors related to not taking into account the reflections from the surrounding probes in a multi-probe system, and by assuming that the signal measured at each probe is proportional e.g. to an electric field component tangential to the measurement sphere, may have a significant contribution on the overall error

budget in the determination of the radiation pattern of an AUT. Indication of the level of errors due to reflections from the surroundings will be shown later in this thesis for the demonstrator system by means of the traditional reflectivity level analysis.

It is now assumed that the signals measured from each probe port contain both the direct signal from the AUT to the probe and the signals due to scattered fields from the neighboring probes. Multiple reflections between the AUT and the probes are assumed negligible. In this case, in theory, the test zone field compensation discussed in Section 3.3.1 could be used to correctly solve for the Q coefficients of the AUT field. This technique will not be applied in this thesis, but its application on multi-probe systems will be briefly discussed in the following.

The application of the test zone field compensation requires an additional calibration measurement for each applied frequency with an antenna whose radiation pattern is known. This measurement has to provide "a multi-probe system response constant" for each probe port of the multi-probe system against each spherical wave mode required in the characterization of the radiated field of the AUT. The known antenna is rotated and translated appropriately in order to create a sufficient number of different excitations for the multi-probe system [34]. The requirements for an appropriate test zone field calibration measurement shall not be discussed in detail here. Though, one practical requirement is that the volume where the known antenna shall locate during the test zone calibration measurement should at least cover the whole test volume required in the actual AUT measurement.

The multi-probe system response constants can then be used to establish a matrix equation for the unknown Q coefficients of the AUT field as follows: $\bar{W} = \bar{\bar{G}}\bar{Q}$, where the elements of the column vector $\bar{W}$ are the signals measured at the probe ports, and $\bar{\bar{G}}$ is now a matrix with dimension $2L \times J$. It is assumed here that two signals from each measurement locations are available, and this reflects a case where e.g. a dual-port probe is used. The elements of $\bar{\bar{G}}$ are the above-mentioned multi-probe system response constants. It is further noted, that the multi-probe system has to be such that the rank of $\bar{\bar{G}}$ becomes equal to J. The least-squares solution to the presented matrix equation is then found in the manner described earlier in Section 3.4.2.

Influence of conventional probe correction

If it is assumed that only the direct signal from the AUT contributes to the signals measured from each probe port in a multi-probe system, the application of the conventional probe correction discussed in Section 3.3.2 will lead to the correct Q coefficients of the AUT field. In Section 4.2.3 the conventional probe correction is discussed in general. Here, its importance in the multi-probe measurement system [P6] is briefly discussed. First, some assumptions are made. Then the importance of a first-order probe correction is considered and finally the importance of the high-order probe correction is considered.

The need for the conventional probe correction is estimated by assuming, that the measurement distance in the multi-probe system [P6] will be approximately 1 m. It is also assumed for this analysis that the significant currents of an AUT in a typical

test case can be enclosed inside a minimum sphere with the radius of approximately 0.05 m.

A dual-port symmetrically-fed patch antenna is used as a probe in the multi-probe system in question [P6]. It is assumed that the radiation characteristics of this patch antenna correspond approximately to those of the patch antenna examined in [59]. The comparison of the azimuthal mode spectra of the patch antenna in [59] with the simulation models of the probes presented in [P4] reveals that the azimuthal spherical mode content of the symmetrically patch antenna is relatively similar to that of the probe number 2 in [P4]. It may thus be assumed that the results presented in [P4] for the probe number 2 will give a good indication of the significance of conventional probe correction in the multi-probe system described in [P6].

First, the significance of the first-order probe correction is considered. With the above-mentioned assumptions, the ratio ϵ, defined in Section 4.2.3, for the multi-probe system now becomes $\epsilon = 20$. In view of the discussions in Section 4.2.3 and the results presented in [56], the application of the first-order probe correction in this case is evidently unnecessary.

Secondly, the importance of a high-order probe correction is considered. In [P4] errors due to application of the first-order probe correction for a high-order probe are examined by computer simulations. One of the simulation cases presented in [P4] is for an AUT model with $r_0 \approx 1.77\lambda$ and for the measurement distance of 10 λ, and this leads to $\epsilon \approx 22.6$. This value is comparable to that for the spherical multi-probe system ($\epsilon = 20$) assumed above, and it is thus assumed that the errors for this simulation case will be representative for estimating the errors due not performing the high-order probe correction in the multi-probe system. In terms of the figure $10\log_{10}(D_{co,pred}) - 10\log_{10}(D_{co,true})$, the errors in the co-polar directivity of the radiated field of the AUT model in the main beam region are generally less than 0.01 dB in this simulation case with the probe number 2 [P4]. Here, $D_{co,pred}$ and $D_{co,true}$ are the predicted and correct co-polar directivities, respectively. This clearly indicates that a high-order probe correction is not important in practice for a multi-probe system with above-mentioned assumptions.

In summary, if the ratio between the measurement distance and the radius of the minimum sphere of the AUT is in the order of 20, the application of the conventional probe correction is clearly not important in practice. In particular, if the influence of the signals due to scattering from the neighboring probes will not be compensated, correcting for the errors due to not applying the conventional probe correction is most often of secondary importance.

4.3.4 System description

Based on the findings and simulations presented in Section 4.3.3, a demonstrator multi-probe system for radiation pattern measurements of mobile phones is built. This demonstrator system will be described in the following.

Mechanics

A spherical 32-antenna measurement system for mobile phones is set up. A photograph of this antenna measurement system, that is referred to as RAMS (rapid antenna measurement system) is presented in Fig. 4.3.

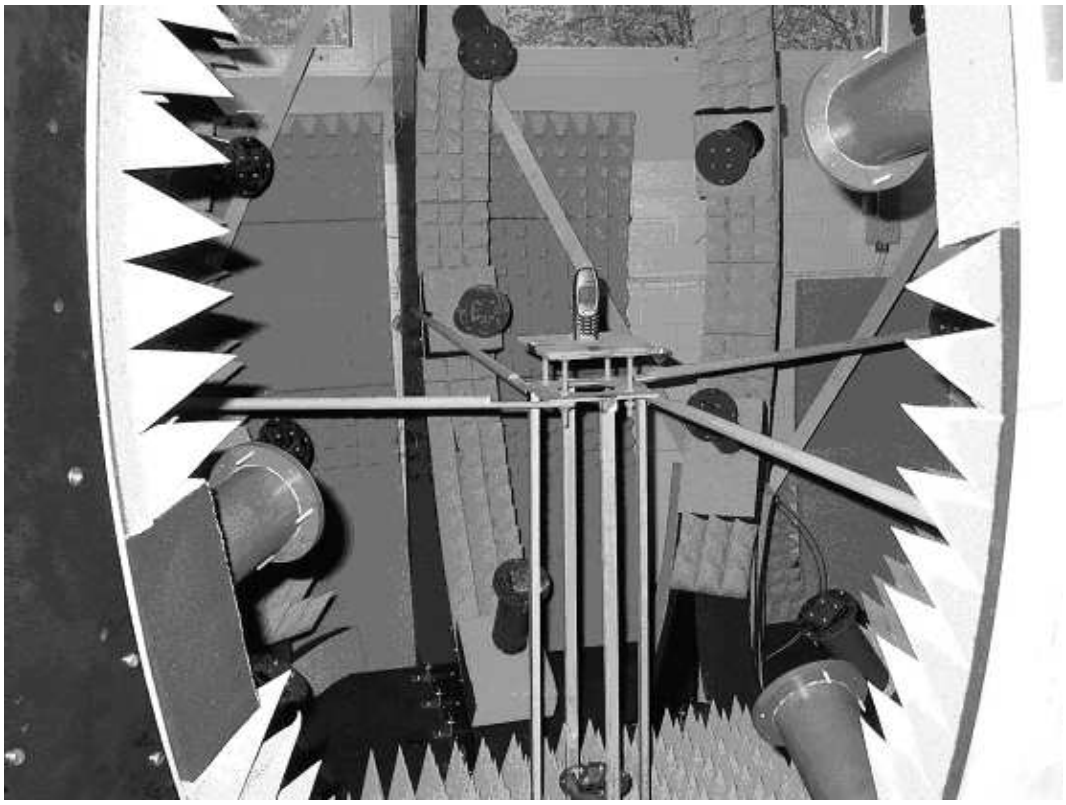

Figure 4.3: Photograph of rapid antenna measurement system (RAMS).

The RAMS consists of the mechanical structure supporting the 32 dual-polarized, symmetrically-fed patch antennas (probes) each of which pointing to the origin of the measurement sphere. The center points of the tangential cross-sections of the probes are located in the corners of concentric virtual icosahedron and dodecahedron as described in [P6]. The distance from the origin of the sphere to the surface of the patch antenna is 0.99 m.

The nominal polarizations of ports I and II of each probe coincide with θ and φ unit vectors, respectively. The ports of the probes are nominally identical, which means that the receiving pattern of the port II corresponds to that of the port I rotated by $\chi = 90°$.

The operating frequency of RAMS is around 1.8 GHz, and mainly limited by the bandwidth of the probes. The far-field criterion of Eq. (2.2) is fulfilled for a normal-size mobile phone at the operating frequency.

Field transformation

It has been earlier decided in Section 4.3.3 that the test zone field compensation approach described in Section 3.3.1 shall not be applied in this work. The studies and analyzes of the significance of conventional probe correction in Section 4.3.3 have further revealed that its application in this multi-probe measurement system [P6] is clearly of secondary importance. Thus, the signals at the ports I and II of each dual-port probe are assumed proportional to the θ and the φ component of the electric field, respectively, on the spherical measurement surface.

All the spherical wave modes up to $n = 4$ are used in the characterization of the radiated field ($N = 4$), and thus the number of spherical wave modes is 48 in total. As the number of samples is 64 in total, and the number of spherical wave modes is 48, the problem is over-determined. The least-squares solution to the Q coefficients of the spherical wave expansion is now found by the application of the matrix method described earlier in Section 3.4.2.

Radio-frequency system

In Fig. 4.4 (a) the radio-frequency system layout of RAMS is illustrated. The system consists of a multiplexing network for conducting altogether 64 radio-frequency signals from the probes to a measurement instrument, which is either a vector network analyzer (VNA) or a spectrum analyzer. The complex radiation pattern measurements for mobile phone models are conducted with the VNA by attaching a feed cable to the model of the mobile phone [P6]. The complex radiation patterns of real mobile phones or mobile phones models without using a feed cable are conducted with the spectrum analyzer [P7].

When RAMS is used with the VNA, the model of the mobile phone is connected to the port I of the VNA with a feed cable. The scattering parameter S_{21} is measured from each measurement channel and the reference channel. By reducing the calibration data from the measured S_{21} values the signals at the probe ports are obtained. The relative field pattern of the radiated far field of the AUT is now obtained by performing the field transformation as described in previous section. The calibration of RAMS is discussed in the following section.

When RAMS is operated in the spectrum analyzer mode, the complex radiation pattern of the AUT is determined without a feed cable to the mobile phone model. The idea is to calculate, separately for each chosen measurement channel, the phase of the measurement channel relative to the phase of the reference channel from the measured amplitude-only data. The hardware necessary for this phase retrieval, shown in Fig. 4.4 (b), constitutes the phase-retrieval network (PRN). After having determined the relative phases of all measurement channels, the relative far-field radiation pattern is obtained using the transformation described in previous section.

Phase-retrieval network (PRN)

The phase retrieval using the PRN is performed by measuring the amplitudes $A_1 = |V_R|$, $A_2 = |V_M|$, $A_3 = |V_R + V_M|$ and $A_4 = |V_R + V_M(\phi)|$, where V_R, V_M and $V_M(\phi)$

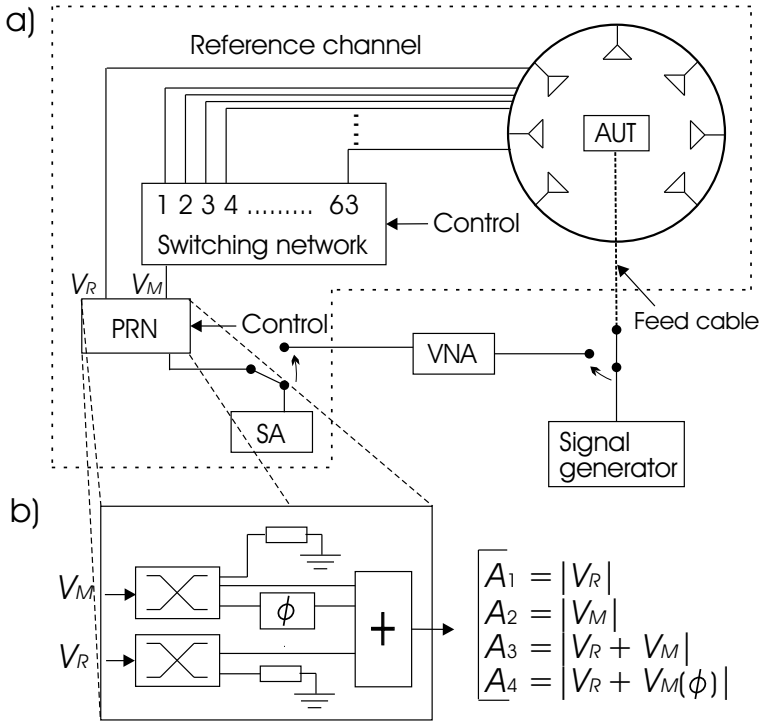

Figure 4.4: Layout of the radio-frequency system of RAMS.

are the signal of the reference channel, the signal of the non-phased measurement channel, and the signal of the phased measurement channel, respectively, and ϕ represents the difference between the path lengths (attenuation and phase change) of the non-phased and the phased measurement channels. The ϕ, obtained from the calibration data for the non-phased and the phased measurement channels, and the four measured amplitudes (A_1-A_4) are used to calculate the phase of V_M relative to the phase of V_R. This type of phase retrieval, where the signal of the measurement channel is compared with the signal of the reference channel, is well-known, and has been applied e.g. in [60], [61] and [62]. In this work, essentially the same phase-retrieval algorithm as described in [63] is used.

After having determined the relative phases, the relative complex signals at the probe ports of the measurement and reference channels are calculated from the known A_2 and the retrieved relative phase of V_M and A_1, respectively, by using the calibration data for the non-phased measurement channel and the reference channel, respectively. The calibration of RAMS will be discussed in the following section.

The PRN may be applied basically for time-harmonic signals at any frequency provided the phase shift ϕ is appropriate. In theory any value except $\phi = n\times 180°$, where $n = 0, 1, 2, 3...$, would be applicable. A preferable value (intuitively) is $\phi = 90°$, which should enable a robust phase retrieval. It is noted, that the PRN reported in [P7] actually contains two phased measurement channels, both with different phase shifts ϕ, and this PRN has been shown to work on the wide frequency range in [64].

In this work the PRN is applied only for time-harmonic signals. In theory, the phase-retrieval using the PRN is strictly-speaking valid for time-harmonic signals only. It is however estimated here (though without proof) that in practice the PRN

may be applied also for some non-time-harmonic signals, e.g. for GSM signals. The the relative bandwidth of the signal has to be small. This practically means that the PRN may be used only for signals of such real mobile communication systems where the modulation bandwidth is small compared to the operating frequency. Due to the fact that the phase-retrieval is based on measuring amplitudes, it is also required that the amplitude of the signal remains constant during all 4 required amplitude measurements. This means that, generally, the PRN may not be used for amplitude-modulated signals. A further requirement is that the path lengths of the measurement and the reference channels (from the AUT to the receiver) are not significantly different. In practice, this is not typically the case with multi-probe measurement system like RAMS.

4.3.5 System tests

The RAMS will now be tested to validate its correct operation both in the VNA and the spectrum analyzer mode. Some of these tests and test results are reported in [P6] and [P7]. In the following the calibration of RAMS, example results and uncertainties will be discussed.

Calibration

The calibration of RAMS is performed with the VNA. The probes, that are assumed identical, are detached and excluded in the calibration of RAMS. Both in the VNA and the spectrum analyzer mode of RAMS each of the 64 signals from the probes are conducted through the output of the PRN to the measurement instrument as shown in Fig. 4.4. The calibration measurement is therefore performed by connecting the desired measurement or the reference channel to the port I of the VNA and the output of the PRN to the port II of the VNA, and by determining the S_{21} with the VNA. The determined S_{21} value thus represents the attenuation and phase change of the signal when it propagates from a probe port to the output port of the PRN.

When the RAMS is operated in the VNA mode 63 non-phased (V_M) measurement channels through the PRN and the reference channel are used, and the calibration coefficients are thus measured for all these channels. When the RAMS is operated in the spectrum analyzer mode both the non-phased (V_M) and the phased ($V_M(\phi)$) measurement channels through the PRN are used. Therefore, in addition to the calibration coefficients of the non-phased measurement channels and the reference channel, the calibration coefficients are now determined also for the phased measurement channels.

Example results

The test measurements with RAMS are performed for a model of a mobile phone. The results of these measurements and the reference measurement are presented in Fig. 4.5. The obtained radiation patterns in a chosen plane in the VNA and SA mode of RAMS show a relatively good agreement with the radiation pattern measured, for comparison, in the small anechoic chamber. The errors in the amplitude in those

directions where the relative level of the amplitude is high are approximately 2 dB at maximum. The corresponding phase errors are approximately 20° at maximum. The errors may be explained partly by the uncertainties of RAMS, but also partly by the uncertainties of the reference measurement.

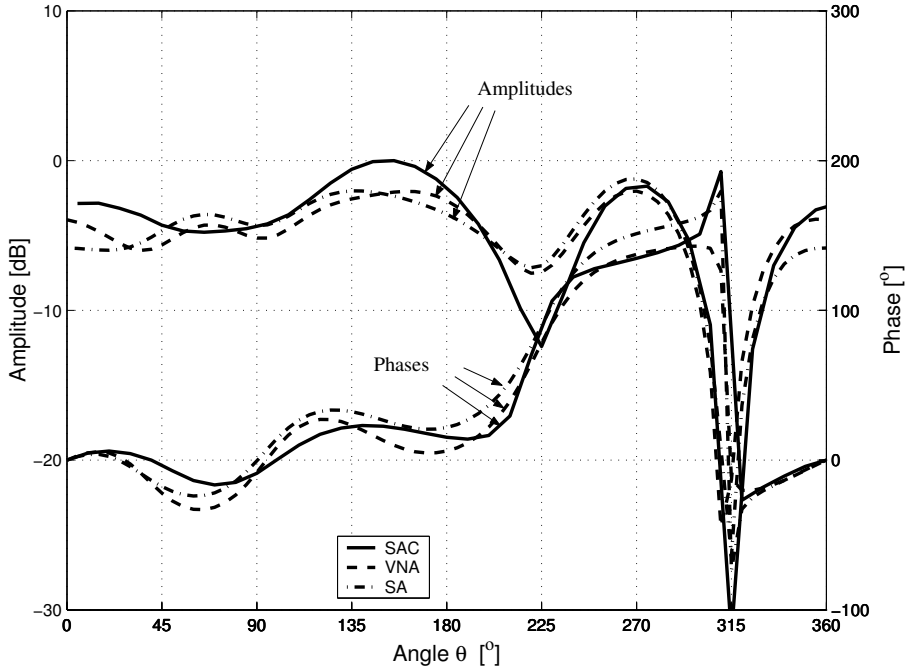

Figure 4.5: The amplitudes and the phases of the electric field radiated by a model of a mobile phone obtained by RAMS in the vector network analyzer mode (VNA) and in the spectrum analyzer mode (SA) compared with the amplitudes and the phases measured in a small anechoic chamber (SAC).

Uncertainties

Uncertainties related to the determination of the radiated fields of mobile phones include e.g. reflections inside RAMS, phase-retrieval errors, drift of the system, uncertainty of the measured power by the spectrum analyzer and the measured s parameter by the VNA, calibration errors, non-similarity of the probes, truncation of the spherical wave series and a small number of measurement locations, multiple reflections between the probe and the mobile phone, and the fact, that the probe correction is not performed. In the following a reflectivity level analysis of RAMS is first carried out. Then, the differences of the complex signals obtained by RAMS in the spectrum analyzer and VNA mode are analyzed. This uncertainty includes e.g. the uncertainties due to phase-retrieval errors, the drift of the system, the uncertainty of the measured power by the spectrum analyzer and the measured s parameter by the VNA. This uncertainty is called the operating mode uncertainty.

The reflectivity level of RAMS is of general interest, and it is assumed to be the main source of uncertainty in the determination of the radiation pattern of a mobile phone. The reflectivity level R is defined as $R = 20\log_{10}\frac{|w_r|}{|w_d|}$, where w_r and w_d are the reflected and the direct signals, respectively, measured at the probe [65]. A $+z$-polarized monopole antenna is moved inside RAMS to 15 different and known

positions in a 3-D space at the distance of not more than about 0.1 m from the origin of the test zone. These positions are denoted by index $p = 1..15$. For each position p, and for port I of each probe, excluding the port I of the reference probe and the probes at $-z$ and $+z$ axes, the transmission coefficient t_{pq}, where $q = 1..29$ denotes the probe port, is measured with the VNA. The obtained values t_{pq} are then corrected to calculate the distance-corrected transmission coefficients t'_{pq} using the assumption that the phase and the amplitude of the signal received by each probe port depend only on the distance between the center points of the monopole and the probe by the function $\frac{e^{jkr}}{kr}$. The direct signal at the probe q is $w_{d,q}$, and it is now assumed to be $w_{d,q} =< t'_{1q}...t'_{15q} >$, where $<>$ denote the mean value. The reflected signals $w_{r,pq}$ for each p and q are thus $w_{r,pq} = t'_{pq} - w_{d,q}$. The 15 reflectivity levels at each probe (R_{pq}) are now $R_{pq} = 20\log_{10}\frac{|w_{r,pq}|}{|w_{d,q}|}$. The root-mean-square (rms) value R_{rms} of the reflectivity levels R_{pq} for $p = 1..15$ and for $q = 1..29$ is then determined as follows: $R_{rms} = \sqrt{\frac{1}{15\times 29}\sum_{p=1}^{15}\sum_{q=1}^{29}|10^{\frac{R_{pq}}{20}}|^2}$. The reflectivity value of RAMS is $R_{RAMS} = 20\log_{10}(R_{rms})$ is then determined. The obtained reflectivity value is $R_{RAMS} \approx -14.8$dB.

It is noted, that the estimation of the reflectivity level in a manner described above is highly sensitive to the uncertainty of the location of the monopole during the measurement, and it results, obviously due this uncertainty, in a relatively high value of R_{RAMS}. Another way of estimating reflectivity, is to calculate, instead of the reflectivity levels R_{pq}, the values of $R'_{pq} = 20\log_{10}\frac{|w'_{r,pq}|}{|w'_{d,q}|}$, where $w'_{d,q} = | < t'_{1q}..t'_{15q} > |$ and $w'_{r,pq} = |t'_{pq}| - |w_{d,q}|$. Further the rms value R'_{rms} is calculated as follows: $R'_{rms} = \sqrt{\frac{1}{15\times 29}\sum_{p=1}^{15}\sum_{q=1}^{29}|10^{\frac{R'_{pq}}{20}}|^2}$. The obtained value R' becomes $R' = 20\log_{10}(R'_{rms}) \approx -22.7$dB. Determination of the value R' is not highly sensitive to the uncertainty of the location of the monopole during the measurement.

The phase-retrieval capability of the system in the spectrum analyzer mode is demonstrated in [P7]. The results from the measurements of the radiated field of a mobile phone model in four orientations indicate that the differences between the measured phase with the VNA and retrieved phase with the spectrum analyzer are within $\pm 7^\circ$ for 90 percent of the directions [P7]. Now, this operating mode uncertainty is analyzed by calculating an rms value of the relative difference signals between the signals obtained in the two operating modes of RAMS as follows. Each of the four measurements of the radiated field of a mobile phone model provide 64 complex-valued signals both for the VNA and spectrum analyzer mode of RAMS. These signals are named $w_{VNA,ol}$ and $w_{SA,ol}$, where $l = 1...64$ indicates the probe port, and $o = 1...4$ indicates the orientation of the mobile phone model, and VNA and SA indicate the VNA and spectrum analyzer mode of RAMS. First, for each fixed o, normalized signals for the spectrum analyzer mode of RAMS are determined as $w'_{SA,ol} = c_o w_{SA,ol}$, where c_o is a complex number which minimizes the sum of the squares of the difference between $c_o w_{SA,ol}$ and $w_{VNA,ol}$ with $l = 1...64$. The error signals are then determined for each fixed o as $w_{e,ol} = w'_{SA,ol} - w_{VNA,ol}$, and the relative error signals as $w_{rel,ol} = \frac{|w_{e,ol}|}{|w_{VNA,ol}|}$. Now, an rms value is calculated as $A_{rms} = \sqrt{\frac{1}{4\times 64}\sum_{o=1}^{4}\sum_{l=1}^{64}|w_{rel,ol}|^2}$, and an error value A is determined as $A = 20\log_{10}(A_{rms}) \approx -15.2$dB.

The error value calculated in the manner described above is strongly influenced by

e.g. the signals whose levels are low relative to the peak signal level. The above calculation is now repeated by including only those signals whose levels are less than 25 dB below the peak signal level. The obtained error value $A_{-25\mathrm{dB}}$ is now $A_{-25\mathrm{dB}} \approx -18.6\mathrm{dB}$.

In theory, the reflections inside RAMS are to a high degree similar for both operating modes of RAMS, and therefore the operating mode uncertainty is practically independent on the reflectivity level of RAMS. These two error sources may thus be treated as two independent error sources. In conclusion, the order of the uncertainty due to reflections and due to the operating mode is approximately the same.

4.3.6 Future prospects for RAMS

At present, there are several issues related to RAMS that could be developed further. These issues include e.g. lowering the uncertainty of the determination of the far field, increasing the speed of the measurement, making the system more wideband, and e.g. the application of advanced methods for the data processing. Some of these are currently underway or have been performed already at Helsinki University of Technology [64]. The listed development possibilities are not completely independent from each other, because e.g. increasing the speed can also potentially lower the uncertainty if the drift of the system is reduced. In the following some of the listed issues are briefly discussed.

The reflections inside RAMS are a major source of uncertainty. The influence of the reflections could be suppressed by the application of the test-zone field compensation technique discussed in Section 3.3.1. This techniques would also compensate for the influence of the non-similarities of the probes. One further possibility to reduce the influence of the reflections would be to use a time-domain measurement discussed in Section 2.6. Another uncertainty is the operating mode uncertainty, comprising e.g. the phase-retrieval uncertainty. This uncertainty could be reduced e.g. by adding extra channels to the phase-retrieval network. Also, the uncertainty caused by the possibility of having a low-level or otherwise inappropriate signal in the reference channel could be reduced e.g. by using more than one reference channel.

The speed of the system is one of the interesting development areas of the system. Here the system could obviously be developed using modern electronics to be practically a real-time system in the frequency domain. The exploitation of a time-domain technique would offer an attractive possibility to develop the system to be basically real-time on the wide frequency range. A real-time system would offer possibilities to analyze instantaneous radiated field of mobile phones. It would also allow to measure numerous radiation patterns in a very short time, and this would offer possibilities for a more reliable estimation of the performance of a mobile phone (model) in numerous user positions.

Advanced data processing methods could offer further possibilities for reducing the uncertainty of the far-field determination. E.g. the IM method [P2] could obviously be applied for RAMS provided the method were formulated for the near-zone case. This method could not only be used to reduce the uncertainty of the determination of the far field, but it could also provide more functionality to RAMS. At present, it is assumed the mobile phone is placed in the center of RAMS, because the origin

of the spherical wave expansion is located there. The application of the IM method for RAMS would allow the mobile phone to be placed within a certain volume near the origin of RAMS without practically increasing the uncertainty of the far-field determination.

4.4 Multiple Spherical Wave Expansions (MSWE) Technique

4.4.1 Introduction

The possibility to use multiple spherical wave expansions for the field characterization is presented in [P8]. The idea is to fully cover the volume of the AUT with a number of virtual spheres of appropriate size, so that the characterization of the radiated field involves spherical waves that evolve from the centers of these virtual spheres. In this way, in view of Eq. (3.2), the total number of spherical wave modes required to characterize the radiated field could be smaller than by using a single-origin spherical wave expansion for the field characterization. An obvious disadvantage of this type of a field characterization technique is that typical orthogonality properties of the spherical vector wave functions [5] may not be taken advantage of in a conventional manner to find the unknown Q coefficients. Matrix method may, however, be applied.

It is successfully shown in [P8] for a model of a mobile phone that the number of spherical functions required to characterize radiated field with a certain sufficient degree of accuracy using multiple spherical wave expansions is smaller compared to the using the traditional, single-origin spherical wave expansion. In this section, the purpose is to show, that not only the number of spherical modes [P8] but also the number of measurement directions may be reduced significantly by using the multi-origin instead of the single-origin SWE.

In the following, the background theory related to the MSWE technique will be first presented in Sections 4.4.2 and 4.4.3. A relatively simple simulation will be then performed to illustrate the usefulness of the application of the MSWE technique compared to the conventional SWE technique, and this will be described in Sections 4.4.4-4.4.7.

4.4.2 Theory

For simplicity the analysis is restricted here to a far-field case. When the essential parts of an AUT affecting its radiation pattern can be fully enclosed with P number of spheres, the total radiated far field may then be expressed in terms of the sum of P spherical wave expansions virtually evolving from the centers of these spheres. Each of these expansions may then be translated into a common reference coordinate system using the known spherical vector wave translations [38].

The translation of a single spherical vector wave mode from its pth ($p = 1...P$) local coordinate system to the reference coordinate system can be written as follows:

$$\boldsymbol{F}^{(3)}_{s'm'n'}(|\boldsymbol{r}-\boldsymbol{r}_p|,\theta,\varphi)=\sum_{s=1}^{2}\sum_{n=1}^{N}\sum_{m=-n}^{n}T^{s'm'n'}_{smn}(\boldsymbol{r}_p)\boldsymbol{F}^{(3)}_{smn}(r,\theta,\varphi), \tag{4.2}$$

where $\boldsymbol{r}$ is the vector from the origin of the reference coordinate system to the far-field observation point ($r=|\boldsymbol{r}|$), $\boldsymbol{r}_p$ is the vector from the origin of the reference coordinate system to the origin of the pth local coordinate system (translation vector), and $T^{s'm'n'}_{smn}(\boldsymbol{r}_p)$ are the coefficients related to the translation. These so-called T coefficients can be derived from the translation and the rotation coefficients of the spherical vector wave functions given in [5]. The local and the reference coordinate systems and the translation vector $\boldsymbol{r}_p$ has been illustrated in Fig. 4.6. Noticeably, the angular spherical coordinates (θ',φ') of the local coordinate system in Eq. (4.2) are marked the same as those of the reference coordinate system (θ,φ) because of the far-field assumption.

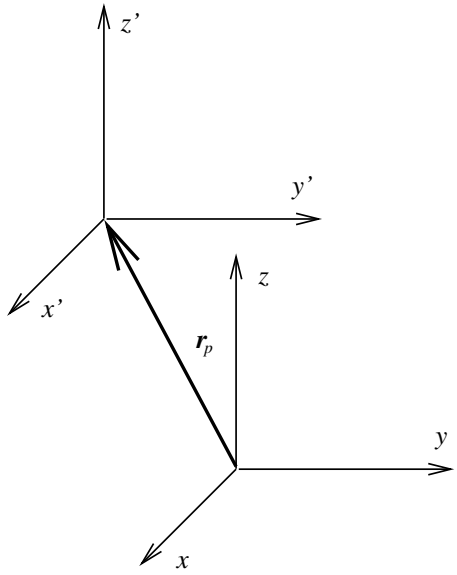

Figure 4.6: The reference (unprimed) and the local (primed) coordinate systems. The x', y' and z' axes are parallel with the x, y and z axes, respectively. Here, the primed coordinates have been used for the local coordinate system, similarly as for the probe coordinate system in Chapter 3.

The multiple spherical wave expansion of the radiated electric far field may now be written as follows:

$$\boldsymbol{E}(r,\theta,\varphi)=\frac{k}{\sqrt{\eta}}\sum_{p=1}^{P}\sum_{s'=1}^{2}\sum_{n'=1}^{N_p}\sum_{m'=-\min(n',M_p)}^{\min(n',M_p)}Q^{(p)}_{s'm'n'}\boldsymbol{F}^{(3)}_{s'm'n'}(|\boldsymbol{r}-\boldsymbol{r}_p|,\theta,\varphi), \tag{4.3}$$

where N_p and M_p are the n' and m'-mode truncation numbers for the pth spherical wave expansion in the pth local coordinate system. Eq. (4.3) may then be written in a shorter form as

$$\boldsymbol{E}(r,\theta,\varphi)=\frac{k}{\sqrt{\eta}}\sum_{p=1}^{P}\sum_{j'=1}^{J_p}Q^{(p)}_{j'}\boldsymbol{F}^{(3)}_{j'}(|\boldsymbol{r}-\boldsymbol{r}_p|,\theta,\varphi). \tag{4.4}$$

Here, Eq. (3.9) and (3.10) form the relation between Eq. (4.3) and (4.4) by replacing indices (s, n, m, j) with (s', n', m', j'), the truncation numbers (N, M) with (N_p, M_p) and the number J with J_p. The J_p thus is the total number of modes in the pth spherical wave expansion.

4.4.3 Matrix method for MSWE technique

Matrix method can be applied also for the case of multiple SWEs. In this case, the matrix $\bar{\bar{F}}_P$, where P indicates the total number of SWEs, is formed as

$$\bar{\bar{F}}_P = \begin{bmatrix} \bar{\bar{F}}_\theta^{(1)} & \dots & \bar{\bar{F}}_\theta^{(P)} \\ \bar{\bar{F}}_\varphi^{(1)} & \dots & \bar{\bar{F}}_\varphi^{(P)} \end{bmatrix}, \tag{4.5}$$

where the block matrices $\bar{\bar{F}}_\alpha^{(p)}$ ($p = 1...P$, and α is θ or φ) are formed from the functions $\boldsymbol{F}_{j'}^{(3)}(|\boldsymbol{r} - \boldsymbol{r}_p|, \theta_l, \varphi_l)$ for $j' = 1...J_p$ and for $l = 1...L$ as follows:

$$\bar{\bar{F}}_\alpha^{(p)} = \frac{k}{\sqrt{\eta}} \begin{bmatrix} \boldsymbol{F}_1^{(3)}(|\boldsymbol{r} - \boldsymbol{r}_p|, \theta_1, \varphi_1)\boldsymbol{u}_\alpha & \dots & \boldsymbol{F}_{J_p}^{(3)}(|\boldsymbol{r} - \boldsymbol{r}_p|, \theta_1, \varphi_1)\boldsymbol{u}_\alpha \\ \vdots & & \vdots \\ \boldsymbol{F}_1^{(3)}(|\boldsymbol{r} - \boldsymbol{r}_p|, \theta_L, \varphi_L)\boldsymbol{u}_\alpha & \dots & \boldsymbol{F}_{J_p}^{(3)}(|\boldsymbol{r} - \boldsymbol{r}_p|, \theta_L, \varphi_L)\boldsymbol{u}_\alpha \end{bmatrix}. \tag{4.6}$$

The Q coefficient vector ($\bar{Q}_P$) for the multiple SWEs case is

$$\bar{Q}_P = \begin{bmatrix} \bar{Q}^{(1)} \\ \vdots \\ \bar{Q}^{(P)} \end{bmatrix}. \tag{4.7}$$

where $\bar{Q}^{(p)} = [Q_1^{(p)}, ..., Q_{J_p}^{(p)}]^{\mathrm{T}}$ for $p = 1...P$.

The least-squares solution to the matrix equation $\bar{\bar{F}}_P \bar{Q}_P = \bar{E}$ is now

$$\bar{Q}_P = (\bar{\bar{F}}_P^{\mathrm{H}} \bar{\bar{F}}_P)^{-1} \bar{\bar{F}}_P^{\mathrm{H}} \bar{E}. \tag{4.8}$$

It is noted, that the measurement locations and also the spherical modes for each of the expansions should be chosen appropriately in order to create a matrix $\bar{\bar{F}}_P$ whose rank is equal to the total number of elements in $\bar{Q}_P$.

4.4.4 AUT model

The AUT model used in this study is described in this subsection. Suppose a radiating structure comprising 4 electric Hertzian dipoles in total. The (x, y, z) coordinates of the dipoles 1-4 are $(0.25\lambda, 0\lambda, 1\lambda)$, $(-0.25\lambda, 0\lambda, 1\lambda)$, $(0\lambda, 0.25\lambda, -1\lambda)$, and $(0\lambda, -0.25\lambda, -1\lambda)$, respectively. The dipoles 1-4 are $+x$, $+x$, $+z$, and $+y$-polarized, respectively, and all of them are excited in phase with the same amplitude.

The locations and the polarization of the dipoles in the reference coordinate system are illustrated in Fig. 4.7. This AUT could represent e.g. an antenna array, whose two radiating elements are at the distance of 2λ from each other.

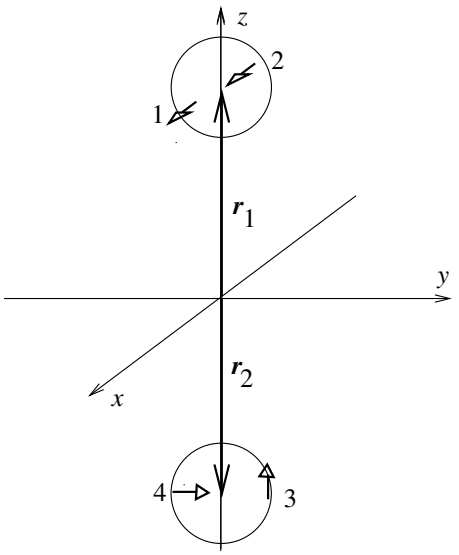

Figure 4.7: The locations and the polarizations of the 4 dipoles (numbered from 1-4) constituting the AUT are illustrated in the reference coordinate system. The dipoles 1-2 and the dipoles 3-4 have been enclosed inside their minimum spheres both of radii 0.25 λ. For later purposes translation vectors $\boldsymbol{r}_1$ and $\boldsymbol{r}_2$ are also marked in the figure.

4.4.5 Number of spherical modes

It will now be tentatively estimated, what is the minimum required number of spherical wave modes for characterizing the radiated field of this AUT using 1) the single-origin spherical wave expansion, and 2) the multiple spherical wave expansions.

According to Eq. (3.2) the truncation number N for the spherical wave expansion of the radiated field of this AUT with $r_0 \approx 2\lambda$ with e.g. $n_1 = 1$ would be $N = 14$. Using the full azimuthal set of spherical vector wave modes this would result in 448 spherical modes in total. However, due to the appropriate choice of the coordinate system relative to the dimensions of the AUT, the AUT may be enclosed inside a cylinder whose radius is $r_c = 0.25\lambda$, and whose axis coincides with the z axis. This allows restricting the m index of the spherical wave expansion to a certain value $m = M < N$. Using Eq. (3.6) with $n_2 = 1$ leads to $M = 3$. From Eq. (3.10), the total number of spherical modes with $N = 14$ and $M = 3$ now becomes $J = 184$. Thus, for $n_1 = n_2 = 1$ using the conventional spherical wave expansion technique leads to 184 spherical modes in total.

Using the double spherical wave expansion ($P = 2$) is an attractive possibility for the field characterization of this particular AUT, because the dipoles 1-2, representing the first radiating element of the array, and the dipoles 3-4, representing the second radiating element of the array, may be enclosed inside their own minimum spheres with radii of $r_{0,p} = 0.25\lambda$, both for $p = 1$ and $p = 2$. The corresponding translation vectors are shown in Fig. 4.7. With $n_1 = 1$, and by replacing $N \rightarrow N_p$ and $r_0 \rightarrow r_{0,p}$ in Eq. (3.2), it now leads to $N_p = 3$ both for $p = 1$ and $p = 2$. It is further assumed that $M_p = N_p$. Thus, using the double spherical wave expansion leads to $\sum_{p=1}^{2} J_p = 60$ spherical modes in total. Here Eq. (3.10) is applied with $J \rightarrow J_p, N \rightarrow N_p$ and $M \rightarrow M_p$.

The above considerations thus suggest that, for the given AUT model, one can potentially benefit from using the multiple spherical wave expansion of Eq. (4.3) instead of a single spherical wave expansion of Eq. (3.7) in trying to minimize the number of measurement locations.

4.4.6 Simulation of an antenna measurement for the AUT model

First, the sampling schemes are decided, and the far field radiated by the AUT model is calculated at sampling directions of each sampling scheme. The electric far field is assumed available for θ and ϕ polarizations equidistantly in θ from 0° to 180° so that the total number of elevation angles is N_θ. For $\theta = 0^\circ$ and $\theta = 180^\circ$ the electric field is assumed available for $\phi = 0^\circ$. For other values of the θ the electric field is available equidistantly in ϕ from 0° to $\frac{360^\circ}{N_\phi}(N_\phi - 1)$, where N_ϕ is the total number of steps in ϕ. In total, 4 different sampling schemes are considered. For the sampling schemes 1-4 the values of N_θ and N_ϕ are $N_\theta = 6, 8, 10$ and 12 and $N_\phi = 5, 7, 9$ and 11, respectively. In this way, the numbers of measurement locations become $L = 22, 44, 74$ and 112, respectively.

Secondly, the truncation numbers (N,M) and (N_p,M_p) for the two characterization methods are chosen for each scanning scheme. For the single spherical expansion method the rank of the matrix $\bar{\bar{F}}$ in Eq. (3.22) has to be equal to J. For the double spherical expansion method the rank of the matrix $\bar{\bar{F}}_P$ in Eq. (4.5) has to equal to $\sum_{p=1}^{P} J_p$. This practically means that for $N_\phi = 5, 7, 9, 11$ both M and M_p are chosen to be $M = M_p = 2, 3, 4, 5$, respectively. Further, $N = 2M$ is an appropriate choice for the single spherical wave expansion in this example case. For the double spherical wave expansion $N_p = M_p$ is applied. For these choices the above-mentioned requirements for ranks of the matrices are fulfilled. As a summary, the total number of spherical modes that used for the single spherical wave expansion technique for sampling schemes with $L = 22, 44, 74, 112$ is $J = 36, 72, 120, 180$, respectively. For the double spherical wave expansion the total number of functions in the characterization for sampling schemes with $L = 22, 44, 74, 112$ is $J_1 + J_2 = 32, 60, 96, 140$, respectively.

Finally, the characterization of the radiated field is performed 1) with single spherical wave expansion technique by applying the matrix method described in Section 3.4.2, and 2) with double spherical wave expansion ($P = 2$) by applying the matrix method described in Section 4.4.3.

4.4.7 Results

After the application of the matrix methods, the predicted Q coefficient vectors for both field characterization techniques ($\bar{Q}$,$\bar{Q}_P$) are known for each sampling scheme. The far fields related to these sets of Q coefficients are then calculated from Eqs. (3.8) and (4.4), respectively. The predicted directivities for the single and double spherical wave expansion cases are then calculated from the known electric fields.

The predicted directivities are compared with the known correct directivity calculated directly from the fields radiated by the AUT model for the single and double spherical wave expansion techniques by calculating $\epsilon_1(\theta, \phi) = 10\log_{10}(D_{pred,1}(\theta, \phi))-$

$10\log_{10}(D_{ref}(\theta,\phi))$, and $\epsilon_2(\theta,\phi) = 10\log_{10}(D_{pred,2}(\theta,\phi)) - 10\log_{10}(D_{ref}(\theta,\phi))$ in 1128 directions on a spherical surface. Here $D_{pred,1}$ and $D_{pred,2}$ are the predicted directivities for the single and double spherical wave expansion techniques, respectively, and the D_{ref} is the correct directivity.

The standard deviations of the 1128 values of $\epsilon_1(\theta,\phi)$ and $\epsilon_2(\theta,\phi)$ are calculated for both characterization techniques and presented against the number of measurement locations in Fig. 4.8.

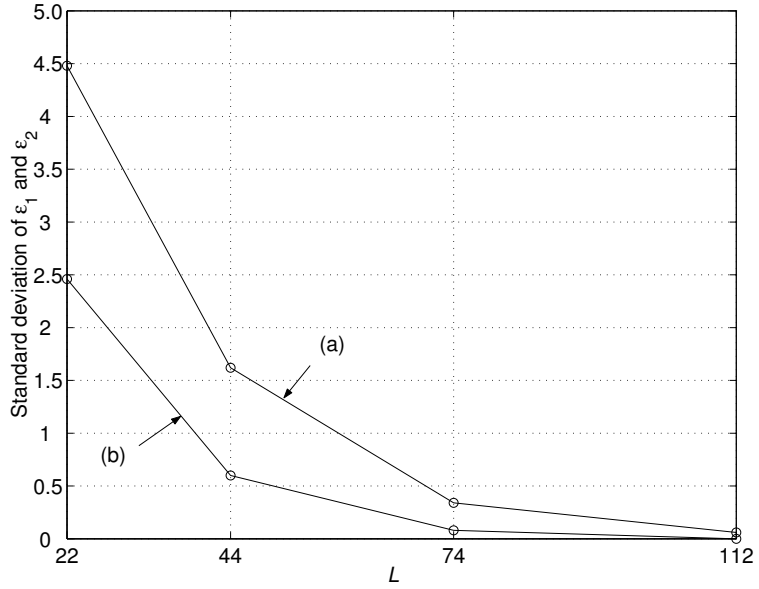

Figure 4.8: The standard deviations of (a) $\epsilon_1(\theta,\phi)$ and (b) $\epsilon_2(\theta,\phi)$ against the number of measurement locations L.

The results presented in Fig. 4.8 clearly illustrate that the double spherical wave expansion technique provides a lower uncertainty in the characterization of the radiation pattern of the AUT model compared to the single spherical wave expansion technique for a certain fixed number L. For example, the standard deviation of the error in directivity for the single spherical wave expansion technique with 44 measurement locations is approximately 1.6 dB whereas it is only approximately 0.6 dB for the double spherical wave expansion technique.

Chapter 5

Summary of publications

In publication [P1] a study on a reasonable truncation number for the spherical vector wave expansion of the radiated field of AUT of relatively small electrical size is carried out by simulations. The results provide information about the errors in the total radiated power and the maximum electric field of an AUT model for a given truncation number and the number of measurement locations as a function of the electrical size of the AUT and the measurement distance. Thus, the results of this study provide a good basis for estimating the minimum number of required measurement locations in the spherical near-zone antenna measurements for electrically relatively small AUT.

In publication [P2] an iterative matrix method is presented for optimizing the number of measurement locations in the spherical far-field antenna measurements. The method is based on iteratively relocating the origin of the spherical vector wave expansion near its nominal origin. The "optimum" origin is found when the difference between the modal field and the measured signals is minimized. The method thus requires that the number of measurements signals is greater than the number of spherical vector wave modes of the modal field.

In publication [P3] the amplitude-only and complex far-field measurements with a relatively small number of measurement locations are compared. The results show that for a fixed and relatively low number of measurement directions, the far field can be characterized more accurately from the complex field samples than from the amplitude-only field samples. The results of publication [P3] further give a suggestion on a reasonable over-sampling factor to be applied in conjunction with the matrix method for solving the spherical vector wave coefficients in noise-free spherical antenna measurements.

In publication [P4] the significance of high-order probe correction for accurate spherical near-field antenna measurements is examined. The spherical near-field antenna measurement is simulated. The signals received by a high-order probe are calculated and the first-order probe correction is applied to these signals. The resulting errors reflect the errors due to high-order azimuthal spherical modes of the probe, which the first-order probe correction is not able to take into account. The results show that the significance of the high-order probe correction increase for an increasing ratio between the minimum sphere of the AUT and the measurement distance.

In publication [P5] the influence of the head phantom on the measurements of the radiated field of mobile phones is examined. The results indicate that by enclosing the head phantom with a mobile phone inside a minimum sphere, and the calculation of the truncation number for the spherical wave expansion of the radiated field based on the radius of this minimum sphere in wavelengths, leads to a clear overestimation of the truncation number. It is suggested that the truncation number is calculated by multiplying the truncation number for a mobile phone without a head phantom by an appropriate factor. In publication [P5] using factor 1.2 is proposed.

In publication [P6] a fully 3-D spherical multi-probe system, consisting of 32 dual-port probes, for measuring radiation patterns of mobile phone models is presented. The system is called RAMS (rapid antenna measurement system). The RAMS allows the radiation pattern be determined without a rotation of the mobile phone. In publication [P6] RAMS is operated with the VNA. The RAMS applies spherical vector wave expansion for the field characterization. The publication [P6] also provides information about the reflectivity level inside RAMS.

In publication [P7] RAMS is equipped with a phase-retrieval network, and it allows to determine the complex radiated field of the mobile phone model from the amplitude-only measurements. It is shown that the complex radiated field can be determined without using a field-disturbing feed cable to the mobile phone model during the measurement.

In publication [P8] a new technique for characterizing radiated fields of antennas is presented with the aim of minimizing the total number of required spherical wave modes in the field characterization. This technique is based on expressing the radiated field with more than one spherical vector wave expansion, so that the origins of the spherical vector wave expansions are in geometrically different locations. The results show that if the total number of spherical wave modes is desired to be restricted to a certain relatively small value, using more than one spherical vector wave expansion can lead to a more accurate characterization of the radiated field compared to using a single spherical wave expansion. In order to show the practical significance of the result presented in [P8], it has been further shown in this thesis that also for a fixed relatively small number of measurement locations the uncertainty in the antenna pattern characterization can be smaller by using multiple spherical wave expansions compared to using a single spherical wave expansion.

Chapter 6

Conclusions

The introduction of the spherical vector wave expansion in [32] provided a basis for later development of the widely-used theory of the spherical near-field antenna measurements presented in [5]. This theory is applicable and useful also for spherical far-field antenna measurements. Today, spherical near and far-field antenna measurements constitute an important, accurate and a widely used technique for measuring radiation patterns of antennas [5] [51].

During the relatively short history of the spherical antenna measurements, single-probe spherical antenna measurement systems have been used extensively. In these systems, the AUT is rotated, often along two rotation axes, and a single probe is used to sample the radiated field in different directions. Anechoic chambers have been built to suppress the reflections from the surroundings. The probe correction theory for spherical near-field antenna measurements has been presented [36], and practical data processing and measurement methods have been developed [40] [41] [42]. Accurate antenna pattern characterization using single-probe systems has thus been based on the assumption of free-space conditions during the measurement, and on the solution of the known analytical relationship between unknown spherical vector wave coefficients of the AUT and the signal measured by the probe.

During the last 10 years spherical multi-probe systems have become common especially in measuring radiation patterns of mobile phones [6]. Spherical multi-probe systems are becoming increasing common in other applications as well [17]. The driving force for the increasing use of multi-probe measurement systems has clearly been the drastic reduction of the measurement time they provide compared to single-probe systems.

This thesis touches upon single-probe and multi-probe spherical antenna measurements. The aims of this thesis have been to deliver concrete guidelines for effectively performing spherical antenna measurements, and to provide theoretical and practical guidelines for designing spherical multi-probe measurement systems.

In this thesis investigations have been performed and techniques developed for minimizing the number of required measurement locations for the determination of the radiated fields of electrically relatively small antennas. Practical guidelines for choosing the truncation number for the field characterization using spherical wave modes have been given. A novel iterative matrix method has been introduced and tested by

simulations. On one hand, this technique enables the minimization of the number of measurement locations in the spherical far-field antenna measurements, and on the other hand, it enables the reduction of the uncertainty of the determination of the radiation pattern. Further, the comparison of the amplitude-only and the complex field measurements for the determination of the radiation patterns has been performed. This comparison indicates that, for a fixed relatively small number of measurement locations, the complex field measurements provide a lower uncertainty in the determination of the radiated field than the amplitude-only measurements.

The significance of probe correction has also been investigated. In general, the results show the importance of the high-order probe correction in spherical near-field antenna measurements. The results show that the high-order probe correction for other than first-order probes becomes increasingly necessary as the ratio between the minimum sphere of the AUT and measurement distance increases.

A new field characterization technique using multiple spherical wave expansions has been proposed. This technique allows to characterize the radiated field with a very small total number of spherical vector modes. It has been further shown in this thesis, that the application of this technique allows reducing the number of measurement locations in testing some AUTs compared to the conventional single spherical wave expansion.

A spherical fully 3-D multi-probe measurement system for mobile phone models has been designed, built and tested. The results successfully show that the complex radiation pattern of a typically-sized mobile phone at 1.8 GHz can be determined with a relatively good and an expected uncertainty without a rotation of the mobile phone using only 32 dual-port probes. The distance from the center of the measurement sphere to the probes is approximately 1 m. The system can be operated with a VNA and a spectrum analyzer. In the spectrum analyzer mode only the amplitudes of the signals are measured. It has been successfully shown that using a phase-retrieval network, the phase is retrievable from the amplitude-only signals with a relatively low uncertainty, and the complex radiation pattern can thus be determined without using a field-disturbing radio-frequency feed cable to the mobile phone model during the measurement. Furthermore, information about the practical uncertainties related to this type of a fully 3-D spherical measurement system have been delivered. For instance, the reflectivity level inside the system has been evaluated, and it is estimated to be in the order of -15 to -20 dB.

The uncertainty of the determination of the far field using a multi-probe system has been partially an unknown issue and a subject of a lot of discussion among the antenna measurement engineers recently. In this thesis, these uncertainties have been investigated. The doubts about the uncertainties have inevitably slowed down the pace by which the single-probe systems are being replaced by the multi-probe systems. In the author's opinion, the trend is however clear. Multi-probe systems systems will be used extensively for antenna testing in future, and not only in e.g. mobile communication applications, but gradually in other applications as well, where the accuracy requirements are clearly higher.

Importantly, the understanding of the possibilities of the test-zone field compensation, proposed e.g. in [34], to compensate the influence of the reflected signals from the neighboring probes in the multi-probe measurement systems is increasing

among the antenna measurement engineers. In theory, the application of a test-zone field compensation technique makes it possible to reach a very low uncertainty level in the determination of the radiation pattern with multi-probe systems. Practical implementation of the these techniques together with the development of effective methods for the test zone field calibration clearly offer an interesting future for the antenna measurement researchers and the antenna measurement community [66].

Bibliography

[1] W. L. Stutzman, G. A. Thiele, *Antenna Theory and Design*, New York, USA, J. Wiley Sons, 1981, 598 p.

[2] C. A. Balanis, *Antenna Theory, Analysis and Design*, New York, USA, 2nd Ed., J. Wiley Sons, 1997, 941 p.

[3] *IEEE Standard Test Procedures for Antennas*, New York, USA, IEEE, Dec. 1979, 143 p.

[4] A. D. Yaghjian, "An overview of near-field antenna measurements," *IEEE Trans. Antennas Propagat.*, Vol. 34, No. 1, 1986, pp. 30–45.

[5] J. E. Hansen, *Spherical Near-Field Antenna Measurements*, London, U.K., Peter Peregrinus, 1988, 387 p.

[6] P. O. Iversen, Ph. Garreau, D. Burrell, "Real-time spherical near-field handset antenna measurements," *IEEE Antennas and Propagations Magazine*, Vol. 43, No. 3, June 2001, pp. 90–95.

[7] S. Saario, D. V. Thiel, J. W. Lu, S. G. O'Keefe, "An assessment of cable radiation effects on mobile communications antenna measurements," *IEEE International Symposium on Antennas and Propagation*, Montreal, Canada, Vol. 1, July 1997, pp. 550–553.

[8] C. Icheln, J. Krogerus, P. Vainikainen, "Use of Balun Chokes in Small-Antenna Radiation Measurements," *IEEE Transactions on Instrumentation and Measurement*, Vol. 53, No. 2, April 2004, pp. 498–506.

[9] C. Braun, G. Engblom, C. Beckman, "Evaluation of antenna diversity performance for mobile handsets using 3-D measurement data," *IEEE Trans. Antennas Propagat.*, Vol. 47, No. 11, Nov. 1999, pp. 1736–1738.

[10] G. J. Foschini, "Layered space-time architecture for wireless communication in a fading environment when using multi-element antennas," *Bell Labs Technical Journal*, Autumn 1996, pp. 41–59.

[11] K. M. Keen, Satellite antenna measurement techniques, *IEE Review*, Vol. 127, No. 7, Sept. 1980, pp. 417–434.

[12] A. Lehto, A. Räisänen, *Mikroaaltomittaustekniikka*, Helsinki, Finland, 5th Ed., Otatieto, 2001, 215 p.

[13] A. C. Newell, R. D. Ward, E. J. McFarlane, "Gain and power parameter measurements using planar near-field techniques," *IEEE Trans. Antennas Propagat.*, Vol. 36, No. 6, June 1988, pp. 792–803.

[14] Z. A. Hussein, Y. Rahmat-Samii, "Application of cylindrical near-field measurement technique to the calibration of spaceborne radar antennas: NASA scatterometer and seawinds," *IEEE Trans. Geoscience and Remote Sensing*, Vol. 37, No. 1, Jan. 1999, pp. 360–373.

[15] O. M. Bucci, M. D. Migliore, "Strategy to avoid truncation error in planar and cylindrical near-field antenna measurement setups," *Electron. Lett.*, Vol. 39, No. 10, May 2003, pp. 765–766.

[16] J. C. Bolomey, B. J. Cown, G. Fine, L. Jofre, M. Mostafavi, D. Picard, J. P. Estrada, P. G. Friederich, F. L. Cain, "Rapid near-field antenna testing via arrays of modulated scattering probes," *IEEE Trans. Antennas Propagat.*, Vol. 36, No. 6, June 1988, pp. 804–814.

[17] J. A. Graham, P.O. Iversen, "Rapid spherical near-field antenna test system for vehicle mounted antennas," *Antenna Measurement Techniques Association, 26th Annual Meeting and Symposium (AMTA'04)*, Stone Mountain, GA, USA, Oct. 2004, PID-130.

[18] L. Duchesne, Ph. Garreau, N. Robic, A. Gandois, P.O. Iversen, G. Barone, "Compact multi-probe antenna test station for rapid testing of antennas and wireless terminals," *10th Asia-Pasific Conference on Communications and 5th International Symposium on Multi-Dimensional Mobile Communications*, Aug. 2004, 553–557.

[19] P. S. H. Leather, J. D. Parsons, "Equalization: a technique to improve the accuracy of antenna radiation pattern measurements," *12th International Conference on Antennas and Propagation (ICAP)*, Mar. 2003, pp. 102–106.

[20] A. D. Olver, "Compact antenna test ranges," *7th International Conference on Antennas and Propagation (ICAP)*, 1991, pp. 99–108.

[21] W. D. Burnside, M. C. Gilreath, B. M. Kent, G. L. Clerici, "Curved edge modification of compact range reflector," *IEEE Trans. Antennas Propagat.*, Vol. 35, No. 2, Feb. 1987, pp. 176–182.

[22] T. H. Lee, W. D. Burnside, "Compact range reflector edge treatment impact on antenna and scattering measurements," *IEEE Trans. Antennas Propagat.*, Vol. 45, No. 1, Jan. 1997, pp. 57–65.

[23] J. Marti-Canales, *Time Domain Antenna Measurments in Compact Ranges and Small Anechoic Chambers*, Ph.D. thesis, European Space Agency, Nov. 2000, 150 p.

[24] T. B. Hansen, A. D. Yaghjian, "Planar near-field scanning in the time domain, Part I: Formulation," *IEEE Trans. Antennas Propagat.*, Vol. 42, No. 9, Sept. 1994, pp. 1280–1291.

[25] T. B. Hansen, "Formulation of spherical near-field scanning for electromagnetic fields in the time domain," *IEEE Trans. Antennas Propagat.*, Vol. 45, No. 4, Apr. 1997, pp. 620–630.

[26] John Kraus, Ronald Marhefka, *Antennas for All Applications*, McGraw Hill, 2002, 960 p.

[27] H. A. Wheeler, "The radiansphere around a small antenna," *Proc. IRE*, Vol. 47, Aug. 1959, pp. 1325–1331.

[28] K. Rosengren, P-S. Kildal, J. Carlsson, O. Lunden, "Measurement of terminal antennas performance in multimode reverberating chambers," *Proceedings of Nordic Antenna Symposium (Antenn'00)*, Lund, Sweden, Sept. 2000, pp. 159–164.

[29] P. Hallbjorner, K. Madsen, "Terminal antenna diversity characterization using mode stirred chamber," *Electron. Lett.*, Vol. 37, No. 5, pp. 273–274.

[30] C. Icheln, P. Vainikainen, P. Haapala, "Application of a GTEM cell to small antenna measurements," *Proceedings of 1997 IEEE AP-S International Symposium and URSI North American Radio Science Meeting*, Montreal, Canada, July 1997, pp. 546–549.

[31] CISPR 16-2, *Specification for radio disturbance and immunity measuring apparatus and methods, Part 2: Methods of measurement of disturbances and immunity*, International Electrotechnical commission, 1st Ed. Nov. 1996, pp. 48–51.

[32] W. W. Hansen, "A new type of expansion in radiation problems," *Phys. Review*, Vol. 47, 1935, pp. 139–143.

[33] R. G. Yaccarino, S. R. Rengarajam, "Application of spherical wave expansion to reflector antennas using truncated field data," *IEEE Trans. Antennnas Propagat.*, Vol. 39, No. 5, May 1991, pp. 639–644.

[34] D. N. Black, E. B. Joy, "Test zone field compensation," *IEEE Trans. Antennas Propagat.*, Vol. 43, No. 4, April 1995, pp. 362–368.

[35] L. Giauffret, D. Bateman, E. Beaumont, P. Garreau, P. O. Iversen, J. C. Bolomey, F. Jensen, "Improved CATR cross polarization performance and antenna pattern error level determination," *ESTEC Contract*, ref. 12878/98/NL/NB, April 2000.

[36] F. Jensen, *Electromagnetic Near-Field Far-Field Correlations*, PhD thesis, LD 15, Electromagnetic Systems, Ørsted·DTU, Tech. Univ. Denmark, Lyngby, Denmark, July 1970, 137 p.

[37] A. D. Yaghjian and R. Wittmann, "The receiving antenna as a linear differential operator: Application to spherical near-field scanning," *IEEE Trans. Antennas Propagat.*, Vol. 33, No. 11, Nov. 1985, pp. 1175–1185.

[38] B. Friedman, "Addition theorems for spherical waves," *Quarterly of Applied Mathematics*, Vol. 12, Apr. 1954, pp. 13–23.

[39] S. Stein, "Addition theorems for spherical wave functions," *Quarterly of Applied Mathematics*, Vol. 19, No. 1, Apr. 1961, pp. 15–24.

[40] P. F. Wacker, "Near-field antenna measurements using a spherical scan: Efficient data reduction with probe correction," *Conference on Precision Electromagnetic Measurements*, No. 113, London, England, 1974, pp. 286–288.

[41] P. F. Wacker, *Non-planar Near-field Measurements: Spherical Scanning*, Report NBSIR 75-809, Electromagnetics Division, Institute for Basic Standards, Nat. Bur. Stds., Boulder, CO, USA, 1975, 55 p.

[42] F. Jensen, "On the probe compensation for near-field measurements on a sphere," *AEÜ*, Vol. 29, No. 7/8, 1975, pp. 305–308.

[43] J. R. James and L. W. Longdon, "Prediction of arbitrary electromagnetic fields from measured data," *Alta Frequenza*, Vol. 38, No. Spec., May 1969, pp. 286–290.

[44] F. H. Larsen, *Probe-corrected Spherical Near-field Antenna Measurements*, PhD thesis, LD 36, Electromagnetic Systems, Ørsted·DTU, Tech. Univ. Denmark, Lyngby, Denmark, Dec. 1980, 157 p.

[45] T. Laitinen, S. Pivnenko, O. Breinbjerg, "Odd-order probe correction technique for spherical near-field antenna measurements," *Radio Science*, vol. 40, RS3009, doi:10.1029/2004RS003063, 2005.

[46] S. L. Campbell and C. D. Meyer, *Generalized Inverses of Linear Transformations*, Dover, New York, USA, 1991.

[47] T. Laitinen, *Spherical Wave Expansion -Based Measurement Procedures for Radiated Fields*, Licentiate thesis, Teknillinen korkeakoulu, Espoo, Finland, Oct. 2000, 71 p.

[48] T. Laitinen, S. Pivnenko, O. Breinbjerg, "Iterative probe correction technique for spherical near-field antenna measurements," *IEEE Antennas and Wireless Propagation Letters*, vol. 4, 2005, pp. 221-223.

[49] T. A. Laitinen, S. Pivnenko, O. Breinbjerg, "On the applicability range of the iterative probe correction technique in spherical near-field antenna measurements," *Antenna Measurement Techniques Association, 27th Annual Meeting and Symposium (AMTA'05)*, Newport, RI, USA, Oct. 30 - Nov. 4 2005, pp. 219-224.

[50] M. S. Bazaraa, H. D. Sherali, C. M. Shetty, *Nonlinear Programming: Theory and Algorithms*, 2nd Ed., Wiley, 1993.

[51] URL: http://www.mi-technologies.com

[52] URL: http://www.nearfield.com

[53] W. J. Wiscombe, "Improved Mie scattering algorithms," *Applied Optics*, May 1, 1980, pp. 1505–1509.

[54] D. A. Hill, "Spherical-wave characterization of interior and exterior sources," *1998 IEEE International Symposium on Electromagnetic Compatibility*, Denver, Colorado USA, Aug. 1998, pp. 848–853.

[55] P. J. Wood, "The prediction of antenna characteristics from spherical near field measurements, part I theory," *Marconi Review*, Vol. 40, No. 204, 1977, pp. 42–68.

[56] M. S. Narasimhan, S. Christopher, K. Varadarangan, "Modal behavior of spherical waves from a source of EM radiation with application to spherical scanning," *IEEE Trans. Antennas Propagat.*, Vol. AP-33, No. 3, Mar. 1985, pp. 350–354.

[57] A. D. Yaghjian, "Approximate formulas for the far field and gain of open-ended rectangular waveguide," *IEEE Trans. Antennas Propagat.*, Vol. AP-32, No. 4, Apr. 1984, pp. 378–384.

[58] K. Kalliola, H. Laitinen, L. Vaskelainen, P. Vainikainen, "Real-time 3-D spatial-temporal dual-polarized measurement of wideband radio channel at mobile station," *IEEE Transactions on Instrumentation and Measurement*, Vol. 49, No. 2, Apr. 2000, pp. 439–448.

[59] T. A. Laitinen, S. Pivnenko, O. Breinbjerg, "Aspects of probe correction for odd-order probes in spherical near-field antenna measurements," *Antenna Measurement Techniques Association, 26th Annual Meeting and Symposium (AMTA'04)*, Atlanta, GA, USA, Oct. 17-22 2004, pp. 98-103.

[60] J. Tuovinen, A. Lehto, A. Räisänen, "Phase measurements of millimetre wave antennas at 105-190 GHz with a novel differential phase method," *IEE Proceedings-H*, Vol. 138, No. 2, Apr. 1991, pp. 114-120.

[61] G. Castaldi, I. M. Pinto, "Well-posed well-conditioned phase-retrieval technique using a known reference source," *IEEE International Symposium on Antennas and Propagation*, Salt Lake City, UT, USA, Vol. 3, July 2000, pp. 1780–1782.

[62] Y. S. El-Said, A. M. Attiya, "Modified two-probe approach for amplitude only near-field measurements," *21th National Radio Science Conference*, Mar. 2004.

[63] J. Berenguer, *Measurements of Radiation Patterns of Mobile Phones in a Small Anechoic Chamber*, Master's thesis, Teknillinen korkeakoulu, Espoo, Finland, Aug. 2001, 64 p.

[64] J. Toivanen, T. A. Laitinen, C. Icheln, P. Vainikainen, "Spherical wideband measurement system for mobile terminal antennas," *2nd IASTED International Conference on Antennas, Radar, and Wave Propagation (ARP'05)*, Banff, Alberta, Canada, July 19-21, 2005.

[65] J. Appel-Hansen, "Reflectivity level of radio anechoic chambers," *IEEE Trans. Antennas Propagat.*, Vol. 21, No. 4, July 1973, pp. 490–498.

[66] http://www.amta.org